AGU PUBLICATIONS

Water Resources Research

RESEARCH ARTICLE
10.1002/2015WR016923

Key Points:
- A framework was proposed to investigate the human effects on TWS
- This framework integrates satellite observation with hydrological modeling
- This framework considers the feedback between human water use and climate variation

Correspondence to:
Y. Huang,
Y.Huang-1@utwente.nl

Citation:
Huang, Y., M. S. Salama, M. S. Krol, Z. Su, A. Y. Hoekstra, Y. Zeng, and Y. Zhou (2015), Estimation of human-induced changes in terrestrial water storage through integration of GRACE satellite detection and hydrological modeling: A case study of the Yangtze River basin, *Water Resour. Res.*, *51*, 8494–8516, doi:10.1002/2015WR016923.

Received 12 JAN 2015
Accepted 7 OCT 2015
Accepted article online 12 OCT 2015
Published online 28 OCT 2015

Estimation of human-induced changes in terrestrial water storage through integration of GRACE satellite detection and hydrological modeling: A case study of the Yangtze River basin

Ying Huang[1,2,3], Mhd. Suhyb Salama[1], Maarten S. Krol[2], Zhongbo Su[1], Arjen Y. Hoekstra[2], Yijian Zeng[1], and Yunxuan Zhou[3]

[1]Department of Water Resources, Faculty of Geo-Information Science and Earth Observation, University of Twente, Enschede, Netherlands, [2]Department of Water Engineering and Management, Faculty of Engineering Technology, University of Twente, Enschede, Netherlands, [3]State Key Lab of Estuarine and Coastal Research, East China Normal University, Shanghai, People's Republic of China

Abstract Quantifying the human effects on water resources plays an important role in river basin management. In this study, we proposed a framework, which integrates the Gravity Recovery and Climate Experiment (GRACE) satellite estimation with macroscale hydrological model simulation, for detection and attribution of spatial terrestrial water storage (TWS) changes. In particular, it provides valuable insights for regions where ground-based measurements are inaccessible. Moreover, this framework takes into account the feedback between land and atmosphere and innovatively put forward several suggestions (e.g., study period selection, hydrological model selection based on soil moisture-climate interactions) to minimize the uncertainties brought by the interaction of human water use with terrestrial water fluxes. We demonstrate the use of the proposed framework in the Yangtze River basin of China. Our results show that, during the period 2003–2010, the TWS was continually increasing in the middle and south eastern reaches of the basin, at a mean rate of about 3 cm yr^{-1}. This increment in TWS was attributed to anthropogenic modification of the hydrological cycle, rather than natural climate variability. The dominant contributor to the TWS excess was found to be intensive surface water irrigation, which recharged the water table in the middle and south eastern parts of the basin. Water impoundment in the Three Gorges Reservoir (TGR) is found to account for nearly 20% of the human-induced TWS increment in the region where the TGR is located. The proposed framework gives water managers/researchers a useful tool to investigate the spatial human effects on TWS changes.

1. Introduction

River basins are substantially influenced by natural climate variability and human activities. With little human activity, hydrological systems are primarily controlled by natural climate variability. As the human population has dramatically increased and many regions experience intensive human activity, human influence can no longer be neglected and should be considered as an important player in the hydrologic cycle [e.g., *Savenije et al*., 2014].

IPCC [2012] has documented evidence, based on observations gathered since 1950, of change in the extremes of, for instance, precipitation and discharge. There is medium confidence that some regions of the world have experienced more intense and longer droughts, whereas, in some regions, there have been statistically significant trends concerning the number of heavy precipitation events. This may relate to indirect human influence on water resources, referring mainly to the effects of anthropogenic changes in climate, which are, for instance, associated with greenhouse gas emissions. Direct human influence is attributed to human alteration of river basins, including but not limited to hydroelectricity generation, irrigation, groundwater abstraction, and land use and cover change (LUCC). On the one hand, human activity can have a large amount of benefits. For example, man-made reservoirs can prevent floods, ease droughts, and generate electricity; irrigation can increase crop production. On the other hand, they commonly affect the distribution, quantity, and chemical quality of water resources and are therefore very likely to have adverse effects. For instance, it is prevalent that increasing water withdrawal worsens water scarcity conditions in semiarid

and arid regions (e.g., Pakistan, India, northeastern China, the Middle East, and North Africa), increasing uncertainties in sustainable food production and economic development [*Hanasaki et al*., 2008b; *Kummu et al*., 2010; *Vörösmarty et al*., 2010; *Wada et al*., 2011b]. Moreover, water impoundment, for instance, in the Three Gorges Reservoir (TGR), can cause a large mass redistribution of water in a short period, likely leading to groundwater recharge and contamination [*Wang et al*., 2011]. Therefore, quantifying the relative effects of natural and human influences on river basins is essential for water management.

In recent decades, a number of macroscale hydrological models have been developed and continuously improved, in order to analyze the effects of human actions on water resources at large scales. *Alcamo et al*. [2003a, 2003b] developed the global water resources and use model WaterGAP and estimated the water withdrawals and availability at a global scale. *Döll et al*. [2009] used the WaterGAP Global Hydrological Model (WGHM) to estimate and analyze globally the river flow alterations due to water withdrawals and reservoirs. Furthermore, *Döll et al*. [2012] used WGHM to estimate the impact of water withdrawals on continental water storage variations. *Hanasaki et al*. [2008a, 2008b] developed the integrated water resources assessment model H08 to stimulate both natural and anthropogenic flows of water globally. Due to the fact that few of these efforts had addressed the issue of human impact on the terrestrial water cycle by explicitly representing them within the framework of land surface models (LSMs), *Pokhrel et al*. [2011] developed an integrated modeling framework (MATSIRO) for assessing the impact of anthropogenic water regulation on surface energy balance. Furthermore, *Wada et al*. [2014] substantially improved the PCR-GLOBWB model [*Wada et al*., 2010, 2011a, 2011b; *van Beek et al*., 2011] by, for instance, explicitly taking into account the mutual feedback between water supply and demand. These models are very valuable to analyze the human perturbation on global water resources; however, they have their own deficiencies and may contain large uncertainties at a regional scale. For example, *Pokhrel et al*. [2011] pointed out that there are certain limitations in their model, including the lack of explicit representations of water table dynamics, water diversions, and evaporation from large reservoirs. Moreover, WGHM does not consider the mutual feedback between human water use and terrestrial water fluxes. In addition, as documented by *Wada et al*. [2014], the improved PCR-GLOBWB model is limited to semiarid and arid regions and unable to reproduce changes in the distribution within countries.

Several studies have tried to analyze, at a regional scale, the effects of human actions on water resources, by comparing the simulated naturalized situation of the hydrological system with the real situation [*Barco et al*., 2010; *Lorenzo-Lacruz et al*., 2010; *Mair and Fares*, 2010]. Furthermore, *van Loon and van Lanen* [2013] proposed an observation-modeling framework to make the distinction between water scarcity (human causes) and drought (natural causes). This framework gives water managers a useful tool to separate natural and human effects on the hydrological system. However, there are some limitations and issues. First of all, it cannot be used in data-scarce regions, because the basic requirements of the framework are the observed data: meteorological data for the entire period, hydrological data for the period without human influence, and hydrological data for the period with human influence. Second, the framework is not suitable for large basins with high geographic diversity, because it does not provide information about changes in spatial distribution of hydrological variables. One possible scenario is that the spatial human effects are cancelled out at basin scale, which gives water managers the illusion of an absence of human effects on the hydrological system. Third, strategies are needed to address the uncertainties introduced by the feedback between human water use and terrestrial water fluxes. These uncertainties include two main parts. The first part is that the observed meteorological data are influenced by human actions. For instance, *Pokhrel et al*. [2011], *Lo and Famiglietti* [2013], and others have documented that irrigation alters the surface energy balance, influencing local weather and climate. The second part is the impact of climate variability on human actions. For instance, climate variability may change irrigation water demand and consequently affect water withdrawal, allocation, and consumption [*Thomas*, 2008; *Wisser et al*., 2008].

Emerging advances in hydrologic remote sensing fill the gaps in data availability and water monitoring. The Gravity Recovery and Climate Experiment (GRACE) mission [*Tapley et al*., 2004], comprising twin satellites launched in March 2002, offers a valuable tool to measure temporal and spatial terrestrial water storage (TWS) variations. The GRACE data have been used to validate macroscale hydrological models [e.g., *Döll et al*., 2009; *Pokhrel et al*., 2011], or applied to estimate human-induced changes in groundwater storage [e.g., *Rodell et al*., 2009; *Feng et al*., 2013; *Voss et al*., 2013]. However, the GRACE data are mainly used to estimate groundwater depletion or water impoundment in reservoirs rather than groundwater recharge. This

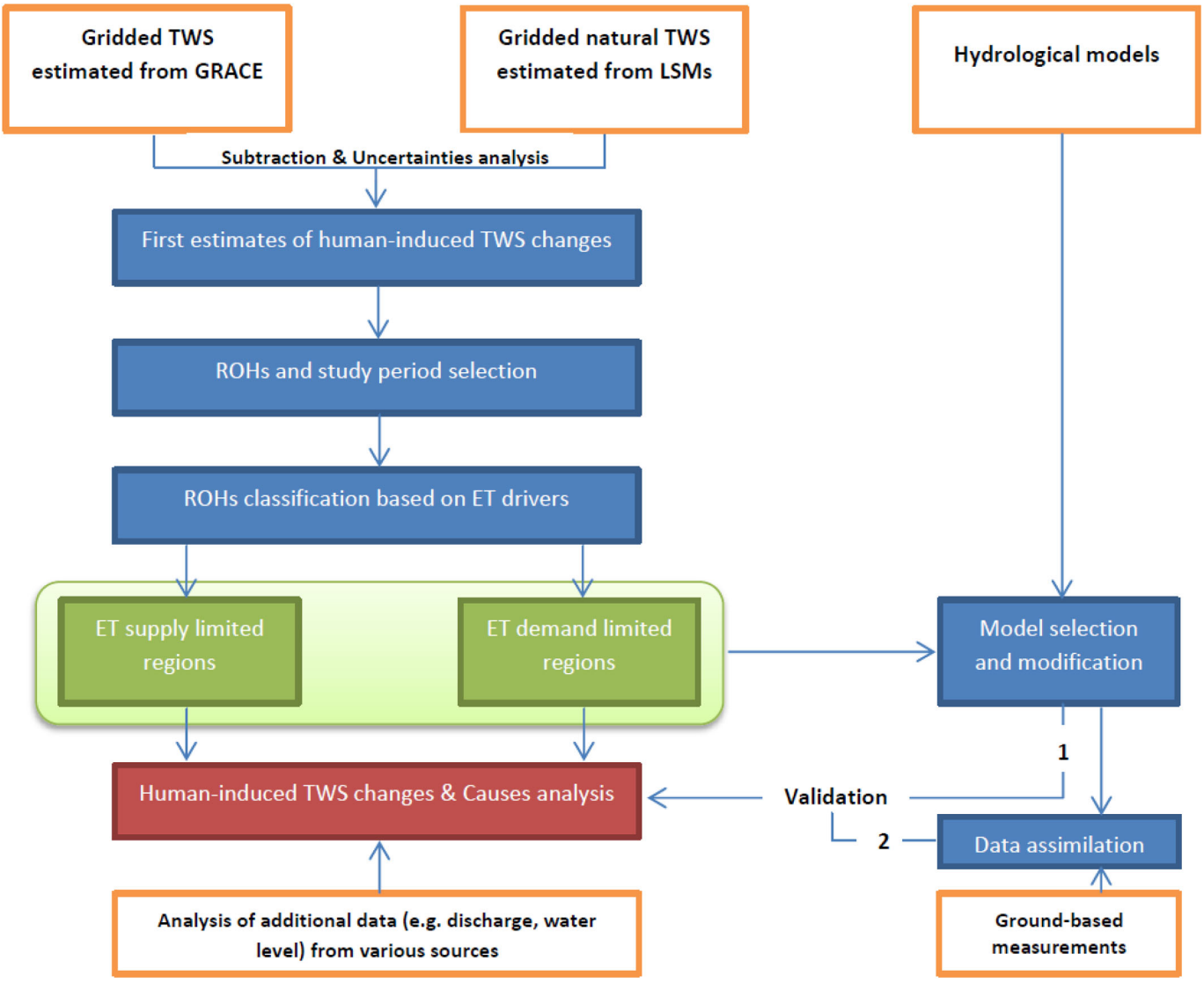

Figure 1. The proposed framework for detection and attribution of spatial TWS changes.

may be attributed to two factors. First, the groundwater recharge caused by, for instance, large-scale irrigation is more complex than groundwater depletion caused by groundwater pumping. The reason for this is that irrigation is influenced by both climate and humans and may alter surface energy balance and hence influence regional climate. Second, the human-induced groundwater recharge at a large basin scale may not be significant enough to attract the attentions of water managers/researchers, and since GRACE data may contain significant errors for relatively small domains, the majority of GRACE applications are still at large scales. The GRACE based groundwater depletion studies did not explicitly consider the uncertainties generated by climate influences on their groundwater depletion estimates, an issue that will be addressed in this paper.

Here we propose a framework, which combines the virtues of GRACE satellite estimation and hydrological model simulation, for detection and attribution of spatial TWS changes. The advantages of this framework are listed as follows. First, the observational data requirement is low, as publicly available data sets are mainly used. Second, it takes into account the feedback between human water use and climate variation. Third, it encourages water managers to, especially for large river basins, locate and analyze regions with observed human effects (ROHs) and further explore the causes, rather than focus solely on basin-average

analysis. This framework integrates GRACE satellite detection with macroscale hydrological modeling and gives water managers and researchers a useful tool to investigate the spatial human effects on TWS in various climate regimes.

This framework is illustrated by its application in the Yangtze River basin. The GRACE data have rarely been applied in a water-rich basin to estimate spatial effects of human-induced changes on TWS mainly caused by large-scale irrigation. The Yangtze River basin experiences intensive human activity. For instance, the basin has been documented as one of the areas with the highest irrigation density in the world [*Siebert et al*., 2005], and intensive irrigation could also have substantial impact on TWS changes [*Döll et al*., 2012; *Long et al*., 2015; *Zhang et al*., 2015]. Although the Yangtze River basin was, in the above-mentioned previous studies, routinely taken as one of the major basins in the world for global water assessment, the human effects on the basin were rarely highlighted or validated by GRACE users and macroscale hydrological modelers. This may be due to the difficulty of resolving the effects of human-induced TWS change on a subbasin scale.

In this study, we first, in section 2, explain the framework for detection and attribution of spatial TWS changes. In sections 3 and 4, the case study area and data are introduced. The application of the framework to the case study area is illustrated in section 5 and discussed in section 6. Finally, the conclusion is drawn in section 7.

2. The Framework for Detection and Attribution of Spatial TWS Changes

The framework designed for detection and attribution of spatial TWS changes is depicted in Figure 1. It integrates two fully independent methodologies, using (1) GRACE satellite data combined with LSMs and (2) macroscale hydrological modeling, to cross-check the estimated human-induced TWS changes.

The left side of Figure 1 shows the method, subtracting LSM estimates from GRACE-observed TWS values, to preliminarily estimate the spatial effects of human-induced changes on TWS (equation (1)), as GRACE data detect TWS changes affected by both climate variability and human activities, whereas LSM simulations represent the climate-related TWS changes.

$$TWS_{human} = TWS_{GRACE} - TWS_{natural}, \tag{1}$$

where TWS_{human} is the estimated human-induced TWS variation, TWS_{GRACE} is the GRACE-derived TWS variation, and $TWS_{natural}$ is the natural part of TWS variation estimated from the LSM. TWS is expressed as equivalent water height (EWH) (cm).

The interannual trend is computed, at each grid, by means of linear regression of the annual mean values of the estimated human-induced TWS. It should be noted that the estimated interannual trend does not explicitly consider seasonal variations, and hence the influence of seasonal variations on the estimated trends needs to be discussed. Uncertainty in interannual human-induced TWS trend is estimated by propagating errors from the GRACE-observed TWS trend and the LSM-simulated TWS trend.

$$\sigma_{h-t} = \sqrt{\sigma_{g-t}^2 + \sigma_{l-t}^2}, \tag{2}$$

where σ_{h-t}, σ_{g-t}, and σ_{l-t} are the uncertainty for human-induced TWS trend, GRACE-based TWS trend, and LSM-simulated TWS trend, respectively. These values are provided by GRACE land products.

Uncertainty in GRACE-derived TWS trend, at each pixel, is computed in two steps: First, we estimate the monthly error of GRACE-derived TWS by using measurement error and leakage error as

$$\sigma_g = \sqrt{\sigma_l^2 + \sigma_m^2}, \tag{3}$$

where σ_g is the error for GRACE-based TWS, σ_l is the leakage error, and σ_m is the measurement error. These values are provided by GRACE land products.

Second, we propagate the monthly error of GRACE-observed TWS onto the least-squares-estimated interannual trend based on *Morrison* [2014] as follows:

$$\sigma_{g-t}=N_{months}*\sigma_g\sqrt{\frac{n\left[n\sum_{i=1}^{n}x_i^2+\left(\sum_{i=1}^{n}x_i\right)^2\right]}{n\sum_{i=1}^{n}x_i^2-\left(\sum_{i=1}^{n}x_i\right)^2}}, \quad (4)$$

where x_i, n, and N_{months} are the sequential data values, the data set record length of the monthly GRACE-based TWS anomalies, and the number of months for 1 year, respectively.

Moreover, uncertainty in LSM-simulated TWS trend (σ_{l-t}), at each pixel, is estimated as the standard deviations of the trends computed from LSMs, as used by *Famiglietti et al*. [2011] and *Voss et al*. [2013] in similar cases:

$$\sigma_{l-t}=\sqrt{\sigma_{e-t}^2+\sigma_{r-t}^2}, \quad (5)$$

where σ_{e-t} and σ_{r-t} are the uncertainties for the employed LSM-simulated TWS trend and the referenced LSM-simulated TWS trend, respectively.

After the preliminary estimates of human-induced TWS changes, several ROHs are selected for further examination. This does allow us not only to explore specific causes at regional scales but also to reduce uncertainties at grid scales, as increasing the size of the region when calculating a regional average generally reduces errors and uncertainties considerably [*Landerer and Swenson*, 2012]. The selection of ROHs is primarily based on the extent of the discrepancy between the GRACE-derived TWS and LSM simulations, hydrometeorological conditions, and types of human activity. The selection of the study period is also an important step in the framework. We selected the period during which the interannual and seasonal variabilities in the estimated TWS from the LSM are rather stationary (natural "stationary" period) for the study. By selecting this period, mathematical artifacts caused by the subtraction of a large positive or negative LSM-simulated TWS trend from the GRACE-derived one can to a certain extent be avoided, and the uncertainties caused by the feedback between human water use and terrestrial water fluxes reduced. More specifically, for the period when the climate is relatively stationary, the change in irrigation water demand related to climate variability is small, and hence the estimates from the method, subtracting the LSM-simulated TWS from the GRACE-derived TWS, largely exclude the uncertainties caused by the influence of climate variability on human activities (e.g., irrigation, water withdrawal, and water consumption).

From a historical perspective, the satellite-based estimates of human-induced TWS are validated by ground-based measurements such as water level measurements. However, these field data are available for only a few regions, and rarely for periods of more than a few years. Besides, in situ observations are point measurements and not always representative for larger spatial domains [*Famiglietti et al*., 2008]. Therefore, modeling of the human effects on TWS changes is a valuable alternative, especially for data-limited regions (Figure 1, the first approach for validation). For the regions with in situ measurements of water levels, it is recommended to apply data assimilation, which combines the virtues of in situ measurements and model simulation of the human effects on TWS, to validate the GRACE satellite-based estimates of human-induced TWS changes (Figure 1, the second approach for validation).

As models have their own deficiencies and limitations, model selection for validation in individual regions is no trivial matter. In order to minimize the uncertainties caused by the feedbacks between human activities and climate variation, information on evapotranspiration (ET) drivers is used to select a hydrological model for validation of ROHs or a certain ROH. *Jung et al*. [2010] and *Seneviratne et al*. [2010] have documented that there is evidence from observations and modeling that, in terms of ET-soil moisture (SM) coupling strength, regions can be roughly classified into two categories: ET supply limited (SM-limited) regions and ET demand limited (energy-limited) regions. In ET supply limited regions, ET is largely governed by the availability of SM, whereas, in ET demand limited regions, ET is mainly controlled by net radiation and not sensitive to SM. As a result, models that consider the effects of human actions on surface energy balance and the potential climate feedbacks should be chosen for ET supply limited regions, since human actions (e.g., irrigation area extension and reservoirs construction) largely change SM, and hence have nonnegligible impact on regional climate. On the other hand, such models may not perform well in ET demand limited

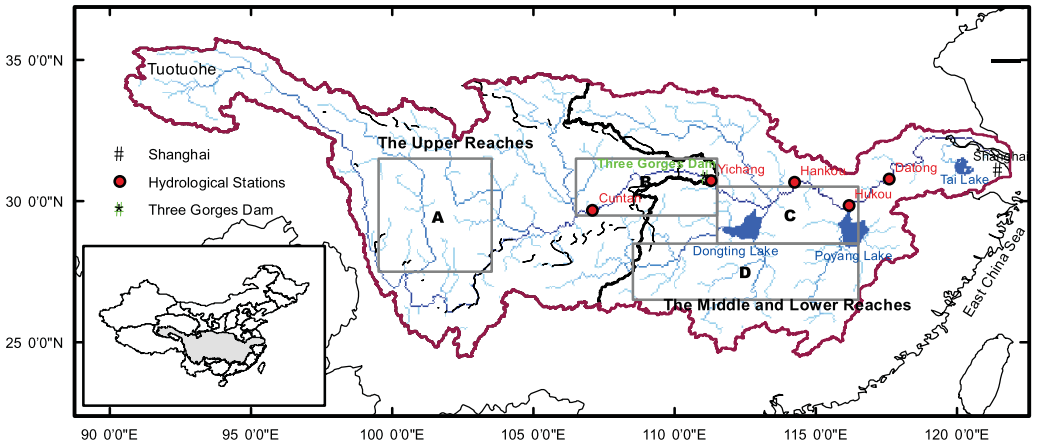

Figure 2. Representation of the study area. The blue polygons, red dots, and green triangle represent the three largest natural lakes (Dongting Lake, Poyang Lake, and Tai Lake), main hydrological stations (Cuntan, Yichang, Hankou, Hukou, and Datong), and the Three Gorges Dam, respectively. Rivers are delineated in blue, and the Yangtze River basin boundary in purple. Squares A–D represent the selected regions, discussed in sections 5 and 6.

regions, because the realistic representations of other processes are more important than land-atmosphere coupling. It should be noted that some regions may switch between ET demand limited and ET supply limited regimes over the course of the year [e.g., *Ryu et al*., 2008] and may also be dependent on land cover [e.g., *Zhang et al*., 2001; *Zaitchik et al*., 2006]. Since we focus on interannual trends of ROHs in this framework, ROHs are classified according to the ET regime dominant during the study period, for which *Jung et al*. [2010, supporting information Figure 2] and *Seneviratne et al*. [2010, Figure 8] offer valuable information.

Previous studies [e.g., *Seneviratne and Stöckli*, 2008; *Teuling et al*., 2009] have illustrated that drivers of ET vary with climate regimes, with a relatively high correlation coefficient of ET and SM in dry regimes, next to a relatively high correlation coefficient of ET and radiation in wet regimes. Despite regional variations, human actions are associated with climate regimes, and hence with ET-SM coupling strength. A large amount of groundwater withdrawal tends to occur in dry regions, whereas surface water is more likely to be predominantly used in wet regions. Therefore, groundwater depletion usually occurs in ET supply limited regions, whereas groundwater recharge caused by surface water irrigation is more likely to take place in ET demand limited regions. These assumptions can be cross-checked in this framework and further supported by auxiliary data (e.g., discharge, lake volumes, and vegetation cover fraction) from various sources.

3. Case Study

3.1. Description of Study Area

The Yangtze River basin, covering 1.8 million square kilometers (km^2), is located in the subtropical zone in China. The river originates in the Qinghai-Tibetan Plateau and flows 6300 km eastward to the sea. The upper Yangtze reaches, the headwaters, extend from the westernmost point, at Tuotuohe, to Yichang. The middle reaches extend from Yichang to Hukou, and the lower reaches extend from Hukou to the river mouth near Shanghai (Figure 2). The climate in the Yangtze River basin is governed by the monsoon, and different climatic systems control the upper and the lower Yangtze River. The amount of annual precipitation (rainfall and snowfall) within the basin tends to decrease inland. Precipitation at the headstream is less than 40 cm yr^{-1}, whereas the lower reaches receive 160 cm yr^{-1}. The wet season from April to October forms a specific weather phenomenon in the middle and lower reaches, and 85% of the annual precipitation occurs during this period.

As also shown in Figure 2, Cuntan, Yichang, Hankou, and Datong are four main hydrological gauging stations located along the mainstream of the Yangtze, receiving discharge from catchment areas of 0.86, 1.01, 1.49, and 1.80 $\times$ 10^6 km^2, respectively. Cuntan forms the entrance to TGR, which extends more than 600 km along the mainstream of the Yangtze River. Yichang is located 37 km downstream from the Three Gorges Dam (TGD), and Hankou is located in the middle reaches of the river. Datong is the gauging station

before the river flows into the sea, and it is used to represent the runoff change in the entire Yangtze River basin.

3.2. Climate and Human Effects

The Yangtze River basin has experienced an increasing trend in the frequency of extreme events, e.g., a marked increase in temperature, low runoff in drought years, and floods during intense rainfall [*Smithson*, 2002]. Moreover, fundamental changes are occurring in this basin, e.g., population growth, economic development, water consumption, as well as dam construction. Therefore, it is interesting and important to study the effects of climate variability and human activity on the Yangtze River basin. *Huang et al*. [2013] investigated the climate-related TWS changes in the Yangtze River basin by analyzing the long-term TWS variations estimated from LSMs, and results have shown that, mainly due to a decrease in the amount of precipitation, the period 2003–2010 is a relatively dry period in terms of TWS in the past three decades. In this study, we focus on the human-induced TWS changes in the Yangtze River basin. More specifically, this study concentrates on the period 2003–2010, during which the climate-related TWS is relatively stationary according to *Huang et al*. [2013, Figure 9], and investigates the human effects on the TWS changes through integration of two fully independent methodologies. The first is based on GRACE satellite observation and LSM simulations. The second method is based on hydrological model simulations to quantify the effects of human actions on water resources.

4. Data

4.1. GRACE

The GRACE Tellus land products, providing monthly TWS variations with spatial sampling of 1°, have been processed by the Center for Space Research (CSR, University of Texas, USA), Jet Propulsion Laboratory (JPL, NASA, USA), and German Research Centre for Geosciences (GFZ, Potsdam, Germany) and are freely available at the website ftp://podaac-ftp.jpl.nasa.gov/allData/tellus/L3/land_mass/RL05/netcdf/. The data are based on the RL05 spherical harmonics from CSR, JPL, and GFZ and have additional post processing steps, summarized online at ftp://podaac-ftp.jpl.nasa.gov/allData/tellus/L3/land_mass/RL05/netcdf/. We used 96 months, from January 2003 to December 2010, of the GRACE Tellus land data computed by CSR. Due to the postprocessing of GRACE observations, surface mass variations at small spatial scales tend to be attenuated. Therefore, it is necessary to multiply those GRACE Tellus land data by the scaling grid provided by JPL. The scaling grid is a set of scaling coefficients, one for each 1° bin of the land grids and is intended to restore much of the signal removed by the post processing steps, such as destriping, filtering, and truncation described in *Landerer and Swenson* [2012].

4.2. Land Surface Model Simulations

In this study, we used two TWS estimates (Noah-MP and ERA-Interim/Land) simulated from different LSMs to double examine the effects of climate variability. We conducted the TWS simulation of Noah-MP, while the outputs of ERA-Interim/Land were obtained online. These two simulations are fully independent of each other, since the two models have different land surface parameterizations and were driven by different forcing data sets. In addition, the Global Land Data Assimilation System (GLDAS) Noah model simulated TWS was used to evaluate the uncertainties in Noah-MP and ERA-Interim/Land simulations.

4.2.1. Noah-MP

Noah-MP was enhanced from the original Noah LSM through an addition of improved physics and multiparameterization options [*Niu et al*., 2011; *Yang et al*., 2011]. It separates the vegetation canopy from the ground surface rather than treating the surface layer as a bulk layer as Noah V3 does and introduces a semitile scheme to represent land surface heterogeneity, which computes shortwave radiation transfer through a modified two-stream radiation transfer scheme [*Yang and Friedl*, 2003; *Niu and Yang*, 2004] considering the 3-D structure of the canopy. A Ball-Berry type stomatal resistance scheme [*Ball et al*., 1987; *Collatz et al*., 1991, 1992; *Bonan*, 1996; *Sellers et al*., 1996], which is related to photosynthesis, and a short-term leaf dynamic model are available in Noah-MP. Moreover, a physically based three-layer snow model [*Yang and Friedl*, 2003], a frozen soil scheme that produces a greater soil permeability [*Niu and Yang*, 2006], and a simple groundwater model with a TOPMODEL-based runoff scheme [*Niu et al*., 2005, 2007] were integrated into the Noah LSM.

In this study, we used the fully augmented version, which has been recommended by default, to simulate the TWS, which includes total column SM (four layers of 0–10, 10–40, 40–100, and 100–200 cm), snow water

equivalent, canopy water storage, and groundwater. This simulation was driven by a $0.1^\circ \times 0.1^\circ$, 3-hourly, and near-surface meteorological data set produced by the Institute of Tibetan Plateau Research, Chinese Academy of Sciences (ITPCAS) [*He*, 2010]. The ITPCAS forcing data merged the observations collected at 740 operational stations of the China Meteorological Administration (CMA) to the corresponding Princeton meteorological forcing data [*Sheffield et al*., 2006] to produce near-surface air temperature, pressure, wind speed, and specific humidity. Several previous studies [e.g., *Chen et al*., 2011] have proved that this forcing data set has a high accuracy in China.

Its simulated runoff was validated with observations at main gauging stations in the Yangtze River. Since Noah-MP does not include river routing, we assess the Noah-MP simulation by comparing its spatially averaged time series of runoff for the source region, the upper reaches, and the entire basin of the Yangtze with the measured data from the Cuntan, Yichang, and Datong gauging stations (Figure 3). This procedure is based on *Balsamo et al*. [2009] as follows. First, we computed the accumulated monthly runoff from Noah-MP data at each pixel during the period 2005–2010. We then calculated the spatial-mean of the accumulated monthly runoff (mm) of all pixels located in the source region, the upper reaches, and the entire Yangtze basin. Second, we divided the accumulated monthly discharge (m^3) of the Cuntan, Yichang, and Datong stations by the area of the source region, the upper reaches, and the entire basin, respectively. This is supported by the fact that the Cuntan, Yichang, and Datong stations respectively form the exit points of the source region, the upper reaches, and the entire basin. The Nash-Sutcliffe efficiency (NSE) is 0.62, 0.60, and 0.84 for the Noah-MP-simulated monthly runoff at Cuntan, Yichang, and Datong, respectively. Moreover, the coefficient of determination (R^2) between monthly observed and Noah-MP-estimated runoff is 0.76, 0.68, and 0.90, respectively. It is also shown in Figure 3 that the Noah-MP simulation is capable of capturing the observed temporal pattern of the runoff. All this illustrates the sufficiency of Noah-MP in simulating TWS variations, especially due to the fact that, in this study, we focus on trends rather than absolute values. TWS anomalies were computed by removing the average over the period from January 2004 to December 2009 at each pixel, to compare against GRACE-observed TWS data.

4.2.2. ERA-Interim/Land

The ERA-Interim/Land data set, produced by the European Centre for Medium-Range Weather Forecasts (ECMWF), describes the evolution of the soil (moisture and temperature) and snowpack covering the period from 1979 to 2010 [*Balsamo et al*., 2015]. It is based on the latest ECMWF land surface model, HTESSEL, driven by meteorological forcing from the ERA-Interim atmospheric reanalysis and precipitation adjustments based on the Global Precipitation Climatology Project (GPCP) v2.1. ERA-Interim uses the Tiled ECMWF Scheme for Surface Exchange over land [*Viterbo and Beljaars*, 1995; *van den Hurk et al*., 2000] to simulate heat and water exchanges between land and atmosphere. This system has been confirmed to perform well in certain key aspects (the representation of the hydrological cycle, the quality of the stratospheric circulation, and the consistency in time of the reanalyzed fields) [*Dee et al*., 2011]. ERA-Interim/Land preserves closure of the water balance and includes a number of parameterizations improvements in the land surface scheme with respect to the original ERA-Interim data set [*Balsamo et al*., 2015], which makes it suitable for this study.

The ERA-Interim/Land-estimated TWS was calculated as the sum of total column SM (four layers of 0–7, 7–28, 28–100, and 100–255 cm) and snow depth and does not give a complete description of the water storage as some components are missing in the model structure. Anomalies were computed by removing the average over January 2004 to December 2009 at each pixel, to compare against GRACE-observed TWS data. The ERA-Interim/Land reanalysis data with the spatial resolution of 1° can be freely downloaded from the website http://apps.ecmwf.int/datasets/data/interim_full_daily/. The accuracies and reliabilities of the ERA-Interim-estimated runoff in the Yangtze River basin were assessed by *Huang et al*. [2013]. Moreover, *Balsamo et al*. [2015] showed the quality of ERA-Interim/Land through a comparison with ground-based and remote sensing observations.

4.2.3. GLDAS-Noah

GLDAS supplies users with a model output of "state-of-the-art" land surface schemes created with atmospheric variables that originate from various data sources [*Rodell et al*., 2004]. In this study, we use the model output produced by the Noah land surface scheme [*Rui*, 2011]. These data are available from 1979 to the present. The Noah SM profile includes four layers, namely 10, 30, 60, and 100 cm, from the soil surface

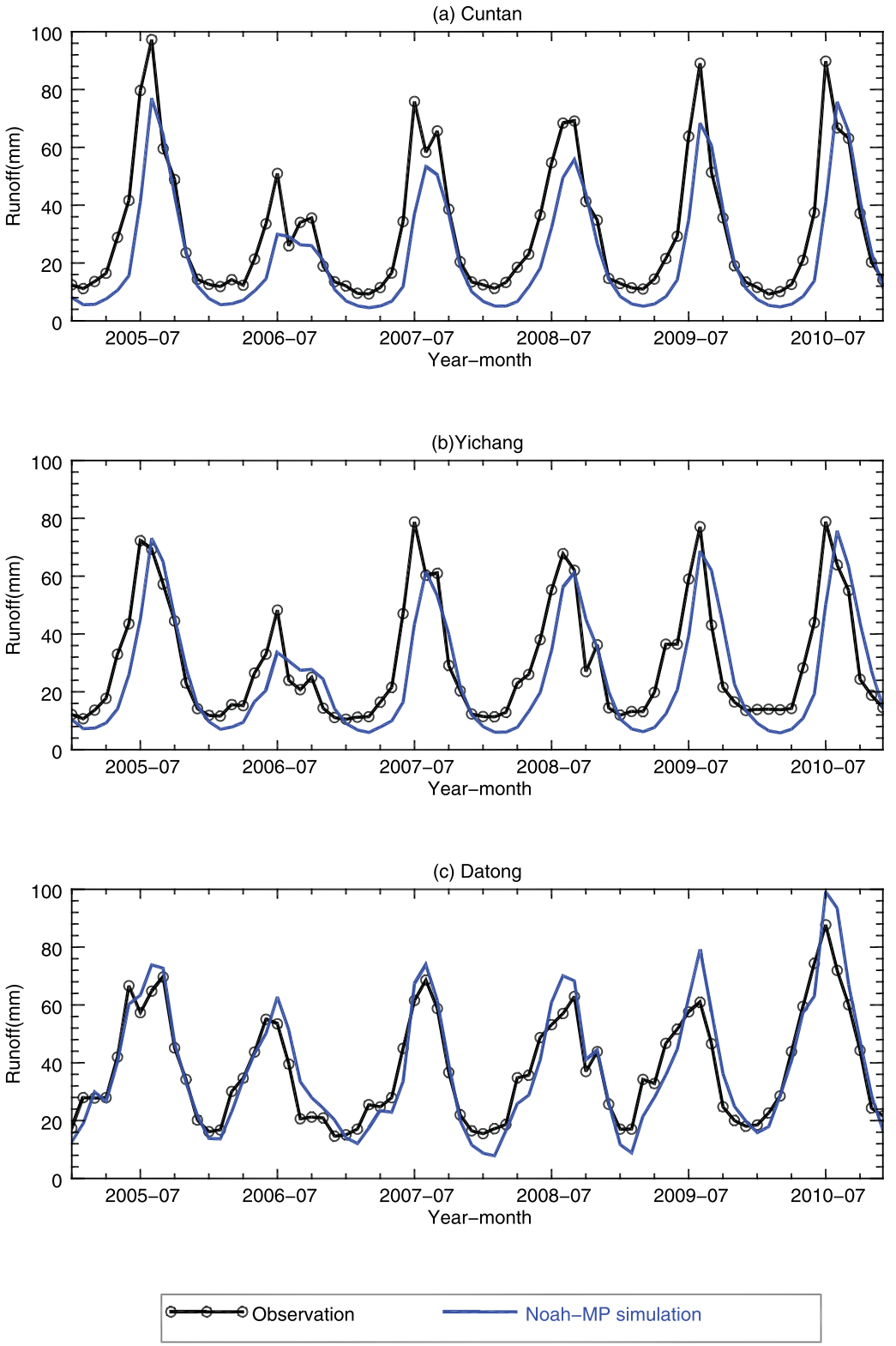

Figure 3. Comparison between the spatially averaged time series of the Noah-MP-simulated monthly runoff for the source region, the upper reaches, and the entire Yangtze River basin during the period 2005–2010 and the measured data from the Cuntan, Yichang, and Datong gauging stations, respectively. Unit: mm.

Table 1. Water Supply, Use, and Consumption in the Yangtze River Basin During the Period 2005–2010 ($\times 10^9$ m^3)[a]

	WU_s	WU_g	WU	WU_i	WU_m	WU_d	WU_e	WU_{gi}	WU_{si}	CU_{gi}	CU_{si}	$(WU-CU)$	NA_g
2005	175.6	7.9	184.2	94.3	64.6	23.2	2.2	4.1	89.9	2.8	34.0	57.1	−36.9
2006	179.7	8.3	188.4	94.3	67.9	23.8	2.5	4.1	90.0	2.9	34.0	57.2	−36.6
2007	185.3	8.1	194.0	93.3	72.9	24.6	3.2	3.9	89.1	2.7	33.7	56.6	−36.4
2008	186.2	8.3	195.2	94.8	71.8	25.1	3.5	4.0	90.5	2.8	34.2	57.5	−36.8
2009	187.9	8.5	197.0	97.0	72.0	26.0	2.0	4.2	92.5	2.9	35.0	58.8	−37.6
2010	189.0	8.5	198.3	94.8	74.7	26.9	2.0	4.1	90.4	2.9	34.2	57.4	−36.6
Mean	184.0	8.3	192.9	94.8	70.6	24.9	2.6	4.1	90.9	2.8	34.2	57.4	−36.8

[a]WU_s is the withdrawal water from surface; WU_g is the withdrawal water from groundwater; WU is the total withdrawal water; WU_i is the withdrawal water from surface water and groundwater used for irrigation; WU_m is the withdrawal water from surface water and groundwater for manufacturing; WU_d is the withdrawal water from surface water and groundwater for domestic; WU_e is the withdrawal water from surface water and groundwater for environment; WU_{gi} is the withdrawal water from groundwater used for irrigation; WU_{si} is the withdrawal water from surface water for irrigation; CU_{gi} is the consumptive water use from groundwater for irrigation; CU_{si} is the consumptive water use from surface water for irrigation; $(WU-CU)$ is the return flow from irrigation to surface water and groundwater; and NA_g is the net abstraction of groundwater.

down. The Noah simulated TWS includes total column SM, snow water equivalent, and canopy water storage.

4.3. Auxiliary Data

For a basin involving intensive human activity such as Yangtze, water supply and consumption data are essential for calculating the impacts of groundwater and surface water use on TWS changes. We used the data of water supply and consumption (Table 1), irrigation area, and fraction of irrigated area that is artificially drained f_d to calculate the return flow from irrigation to groundwater spatially, which serves as the independent TWS estimation compared with those from GRACE and LSM simulations. The yearly water supply data from surface and groundwater, and the consumption data for domestic, manufacturing, irrigation, and environment in this basin were obtained from the Ministry of Water Resources of the People's Republic of China. These data are only available for the period 2005–2010. The Global Map of Irrigation Areas (GMIA) version 5, provided by the global water information system (AQUASTAT) of the Food and Agriculture Organization (FAO), was used to calculate the irrigated area and expressed in hectares per cell [*Siebert et al*., 2013]. Drainage fraction f_d was derived from global-scale information on drainage in rain fed and irrigated agriculture as compiled by *Feick et al*. [2005].

Moreover, the monthly discharge data and the water level variation data of lakes were used to interpret the TWS results. The observed discharge data (m^3 s^{-1}) of main hydrological gauging stations (Cuntan, Yichang, and Datong) in the Yangtze River basin, during the period 2005–2010, were provided by Bureau of Hydrology, Changjiang (also called Yangtze) Water Resources Commission. The monthly water level data for three largest natural lakes (Dongting Lake, Poyang Lake, and Tai Lake) (Figure 2) in the study area were obtained from the web database (HYDROWEB: http://www.legos.obs-mip.fr/en/soa/hydrologie/hydroweb/), developed by LEGOS (Laboratoire d'Etude en Géophysique et Océanographie Spatiale). This database is based on multisatellite altimetry measurements and freely available for the study period [*Crétaux et al*., 2011]. As the time series is not complete for the study period, we used linear interpolation to fill in the missing months.

In addition, the Normalized Difference Vegetation Index (NDVI) and in situ measurements of TWS changes in the TGR were used. The Moderate Resolution Imaging Spectroradiometer (MODIS) derived NDVI product is designed to provide consistent spatial and temporal comparisons of vegetation conditions. The monthly MODIS NDVI during the study period 2003–2010, with a 0.05° spatial resolution, was used as a surrogate for vegetation coverage in this study. The in situ measurements of TGR water volume changes was obtained from the China Three Gorges Corporation (http://www.ctg.com.cn), as used by *Wang et al*. [2011].

5. Application of the Framework to the Yangtze River Basin

5.1. Preliminary Estimates of Human-Induced TWS Variations

We preliminarily applied a linear regression model, at each pixel, to the annual mean values of the satellite estimated human-induced TWS anomalies. Figure 4 illustrates the interannual trends of human-induced TWS variations with the unit of cm yr^{-1} EWH for the period 2003–2010. The trends of human-induced TWS variations obtained from GRACE and Noah-MP (Figure 4a) show a very similar spatial pattern to those

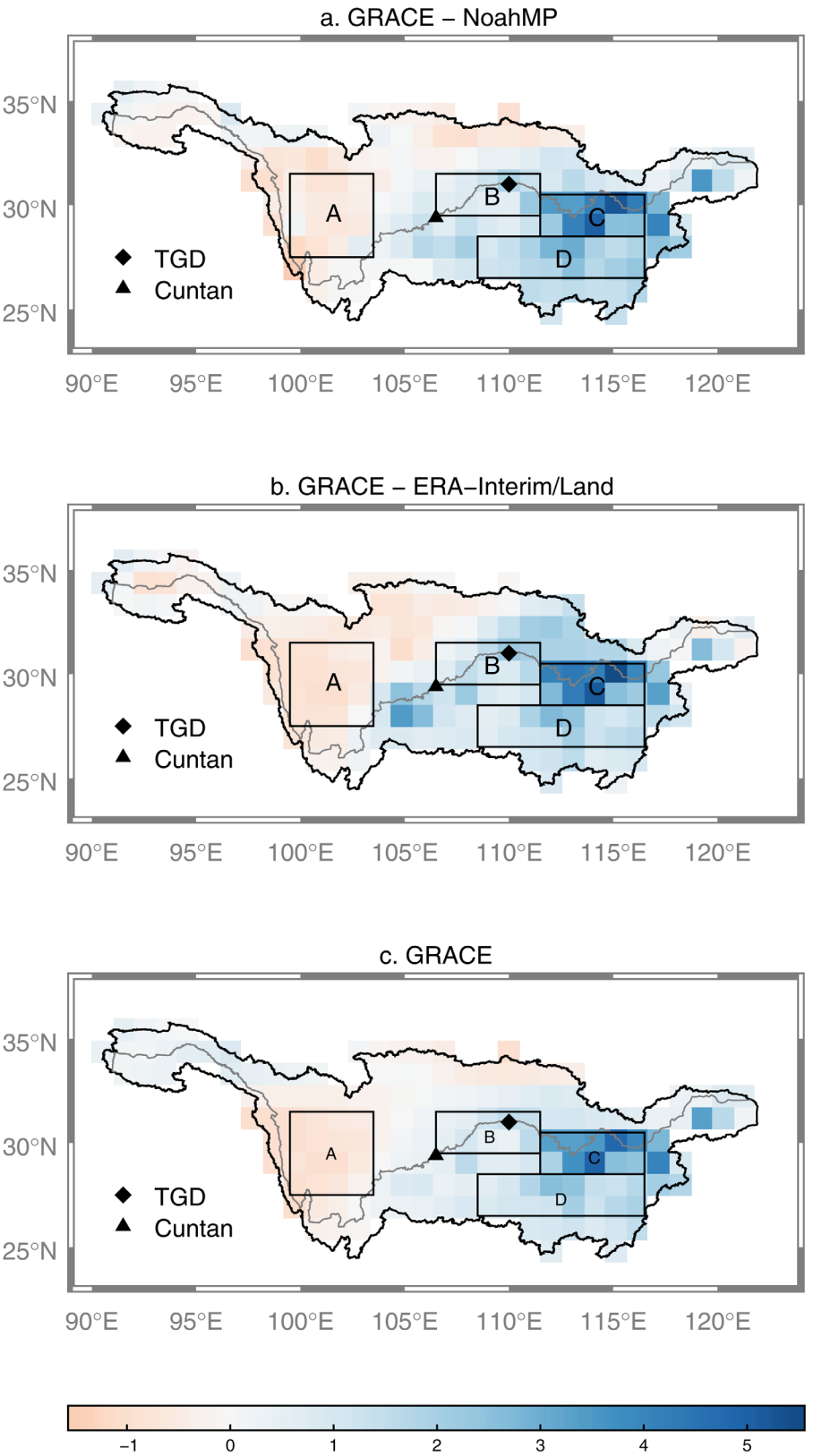

Figure 4. Interannual trends of (a) estimated human-induced TWS from GRACE and Noah-MP simulations, (b) estimated human-induced TWS from GRACE and ERA-Interim/Land reanalysis data, and (c) estimated TWS from GRACE data, with the spatial resolution of 1° in the Yangtze River basin for the period 2003–2010; the gray line represents the Yangtze mainstream. The diamond and triangle represent the location of the TGD and the Cuntan hydrological station, respectively. Squares A–D represent the selected regions. Unit: cm yr^{-1}.

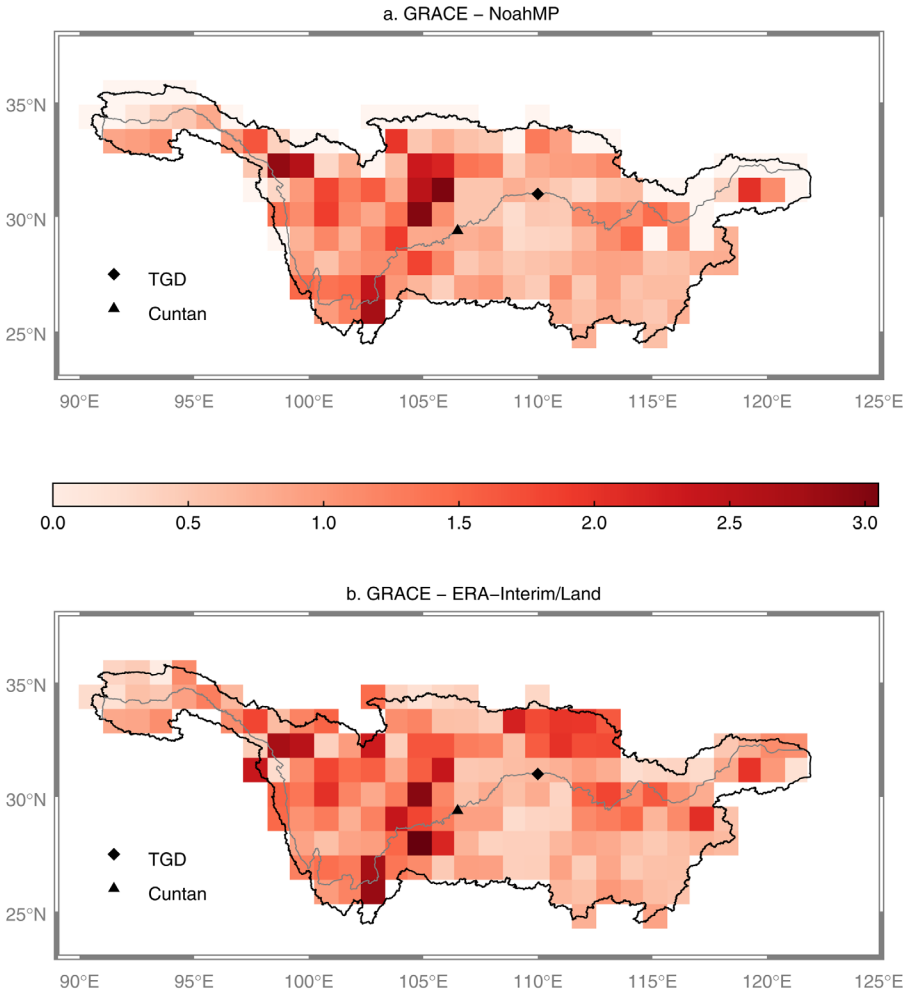

Figure 5. Uncertainties in the annual trends of human-induced water storage based on (a) GRACE and Noah-MP simulations, (b) GRACE and ERA-Interim/Land reanalysis data in the Yangtze River basin. Unit: cm yr^{-1}.

computed from GRACE and ERA-Interim/Land (Figure 4b). This is because they stem from the trends of the GRACE data (Figure 4c), as both Noah-MP and ERA-Interim/Land simulations have no significant trends during the study period. The human-induced TWS shows sharp positive trends in the middle and lower reaches, with a maximum of more than 5 cm yr^{-1}, while a negative trend is observed in the upper reaches. Figure 5 depicts the uncertainties of the human-induced TWS trends of the study area, which are generally larger in the upper reaches of the basin than in the middle and lower reaches. Those uncertainties were estimated by propagating errors from the GRACE-observed TWS trend and LSM-simulated TWS trend (equation (2)). The uncertainties in GRACE-derived TWS trends were computed according to equations (3) and (4). The uncertainties in Noah-MP, ERA-Interim/Land-simulated TWS trends were respectively estimated as the standard deviations of the trends computed from the used LSM and from GLDAS-Noah (equation (5)).

5.2. ROHs and Study Period Selection

Based mainly on the growth rates of the first estimated human-induced TWS changes, we defined the Regions A, B, C, and D as ROHs for further examination (Figure 4). Region A is located in the upper reaches of the Yangtze River basin, while Regions B, C, and D are in the middle and lower reaches (Figure 2). It should be noted that Region B includes the hydraulic basin of China's TGR. The positive GRACE-observed TWS trend of Region B, thus, was affected by the TGR water impoundment [*Wang et al.*, 2011]. Figure 6 shows the spatially averaged monthly time series of the estimated human-induced TWS anomalies in Regions A, B, C, and D. It depicts that, interestingly, the largest human-induced TWS increase occurred in Region C, with a mean rate of 3.7 $\pm$ 0.8 cm yr^{-1} based on GRACE and Noah-MP, and a rate of 3.9 $\pm$ 1.1 cm

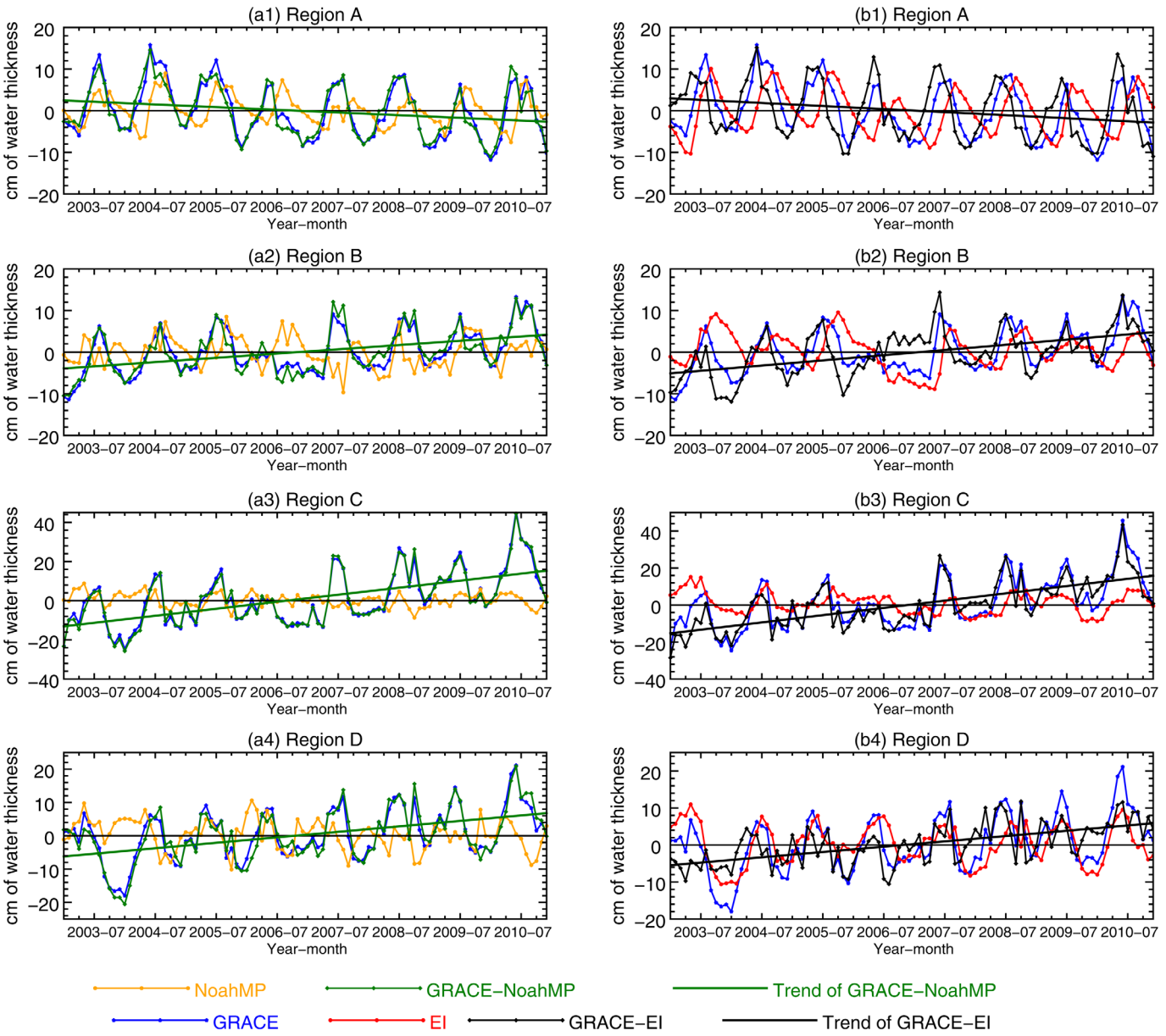

Figure 6. Spatially averaged monthly time series of GRACE-observed TWS (blue star curve), Noah-MP-estimated TWS (orange circle curve), ERA-Interim/Land (EI) estimated TWS (red circle curve), human-induced TWS (green/black diamond curve) variations (as anomalies), and the best fit linear human-induced TWS trend (green/black line) for Regions A–D during the period 2003–2010. The trends of human-induced TWS variations from GRACE and Noah-MP, in Regions A, B, C, and D, are -0.5 ± 0.5, 1.1 ± 1.1, 3.7 ± 0.8, and 1.9 ± 0.7 cm yr^{-1}, and from GRACE and ERA-Interim/Land are -0.7 ± 1.0, 1.3 ± 0.6, 3.9 ± 1.1 and 1.4 ± 0.6 cm yr^{-1}, respectively.

yr^{-1} based on GRACE and ERA-Interim/Land, respectively. Regions B and D experienced smaller water increment during the period 2003–2010. In contrast, there is a small negative trend in Region A. Also shown in Figure 6 is that there is no significant trend in the Noah-MP or ERA-Interim/Land-simulated TWS. Therefore, the period 2003–2010 can be used as study period. Besides, the seasonal variability of the estimated human-induced TWS changes is rather stationary (Figure 6), indicating that, during 2003–2010, seasonal variations have little influence on the computed linear trends.

5.3. ROHs Classification Based on ET Drivers

Jung et al. [2010] and *Teuling et al.* [2009] have estimated the drivers of ET based on model and observational data. *Seneviratne et al.* [2010] have explicitly explained land-atmosphere coupling, the processes controlling ET, and the existence of distinct ET regimes. According to these previous studies, the Yangtze River basin, especially the middle and lower reaches, has consistently been diagnosed as an ET demand limited

regime. This is not surprising, because the climate of the Yangtze River basin is predominantly humid, creating a sufficiently high SM level.

5.4. Validation

Due to the very weak coupling strength between SM and ET, the human activities that change SM (e.g., irrigation) have little impact on ET in the ET demand limited regime. Therefore, the models that consider the feedbacks between land and atmosphere do not have particular advantages. MATSIRO and PCR-GLOBWB 2.0 are two of the most advanced models that take into account the feedbacks between land and atmosphere. However, MATSIRO lacks explicit representations of water table dynamics [*Pokhrel et al*., 2011], and the assumption of PCR-GLOBWB 2.0, using the fraction of daily accumulated base flow to simulate allocation of surface water and groundwater to satisfy the water demands, is unrealistic in humid regions where people predominantly rely on surface water resources [*Wada et al*., 2014]. Additionally, the impact of irrigation return flow was neglected. Therefore, neither is suitable to use for validation in the Yangtze River basin.

In this case study, we select the method of *Döll et al*. [2012] to quantify the impacts of surface water and groundwater withdrawal and consumption on TWS variations. This is due to the fact that, although it does not consider the feedback between human water use and terrestrial water fluxes, or equate water demand with either water withdrawals or consumptive water use, it uniquely estimates water withdrawals according to source, for instance, accounting for the difference between water withdrawals from groundwater and water withdrawals from surface water. For a humid basin like the Yangtze, this hydrological model is therefore suitable for evaluating the impacts of human water use on TWS.

As *Döll et al*. [2012] concentrated on the impact of water use on seasonal variations in TWS rather than trends in the global-scale analysis, and the estimates were based on the data during the period 1998–2002, their modeling results cannot be used to validate the estimated human-induced TWS changes from GRACE and LSMs in this case study. In addition, according to the officially released water use data, water withdrawals are generally used for four sectors: domestic, manufacturing, irrigation, and environment, which are different from the water use sectors defined in *Döll et al*. [2012]. We therefore modified *Döll et al*. [2012, equations (1) and (3)] and recomputed the impact of groundwater and surface water use on groundwater and surface water storages.

Water withdrawals for all sectors and sources results in return flow (*WU* – *CU*) to surface water. It is assumed that the return flow of the irrigation water withdrawn from either surface water or groundwater partly runs off directly to surface water bodies, while the other part recharges groundwater before running to surface water bodies. The water withdrawals for other uses are assumed to directly flow into surface water even if the water source is groundwater. Therefore, the surface and groundwater storages are artificially changed, respectively, by net abstraction of surface water NA_s and net abstraction of groundwater NA_g, which are computed as follows:

$$NA_s = [CU_{sd} + CU_{se} + CU_{sm} + WU_{si}] - [(1 - f_{rgi})(WU_{gi} - CU_{gi} + WU_{si} - CU_{si}) + (WU_{gd} - CU_{gd} + WU_{gm} - CU_{gm} + WU_{ge} - CU_{ge})], \quad (6)$$

$$NA_g = WU_g - [f_{rgi}(WU_{gi} - CU_{gi} + WU_{si} - CU_{si})], \quad (7)$$

where *NA* is net abstraction ($m^3\ yr^{-1}$); *WU* is withdrawal use ($m^3\ yr^{-1}$); *CU* is consumptive use ($m^3\ yr^{-1}$); f_{rgi} is groundwater fraction of return flow from irrigation (*WU* – *CU*), and of the subscripts *g* represents groundwater, *s* represents surface water, *d* represents domestic, *e* represents environment, *i* represents irrigation, and *m* represents manufacturing. It should be noted that net abstractions from groundwater and net abstractions from surface water can be positive or negative. Positive values indicate water storage losses, whereas negative values indicate storage gains. The sum of NA_s and NA_g is equal to consumptive water use. Due to the unavailability of water withdrawal and consumption data for some sectors, only NA_s for irrigation is calculated in this study.

Irrigation *CU* is computed by multiplying irrigation *WU* by irrigation water use efficiencies. We use the default values of irrigation water use efficiencies, 0.378 for surface water use and 0.7 for groundwater use, implemented in WaterGAP for China.

Groundwater recharge is highly dependent on artificial drainage, which causes water to bypass the groundwater store, thus the groundwater fraction f_{rgi} of return flow is calculated as a function of the fraction of irrigated area that is artificially drained f_d:

$$f_{rgi} = 0.8 - 0.6 f_d, \tag{8}$$

where the values 0.8 and 0.6 are taken from *Döll et al*. [2012]. In this study, the spatial yearly return flows are computed by weighting the total yearly return flows from irrigation (*WU – CU*) with the irrigation area percentage (section 4.3), due to a lack of detailed spatial distribution of water supply and consumption data in the study area (Table 1).

As shown in Table 1, a huge amount of water (about 180×10^9 m^3) is used in the Yangtze River basin every year, and approximately 95% of the water supply originates from surface water. Water used for irrigation takes up a large portion of the total water supply, accounting for more than 50% (around 94.8×10^9 m^3) of total water use, while the rest of the water supply is used for domestic, manufacturing, etc.

Figure 7a illustrates that Region C and the river mouth are the most intensive irrigation areas of the Yangtze River basin, and Figure 7b shows that the lower reaches of the basin receive slightly smaller fractions of the return flows from irrigation to groundwater, due to the fact that the lower reaches are more artificially drained. Figure 7c exhibits the spatial pattern of yearly average net abstraction of groundwater (NA_g), which was calculated from the values of irrigation areas, fractions of the return flows (f_{rgi}), and water use and supply data released by the Ministry of Water Resources of China (Table 1). Great negative values in the middle and lower reaches of the basin indicate that large amounts of irrigated water recharged groundwater, especially in Region C. We further computed the spatially averaged time series of net abstraction of groundwater in Regions A, B, C, and D, respectively, as shown in Table 2. In the selected four ROHs, Region C experienced the greatest groundwater gains, with a mean rate of 4.2 cm yr^{-1}. The groundwater also increased in Regions B and D during the study period, but at a lower rate than in Region C, namely 1.2 and 3.0 cm yr^{-1}, respectively.

6. Discussion

In this study, we designed a framework for detection and attribution of spatial TWS changes and took the Yangtze River basin as an example to investigate the spatial effects of human-induced changes on TWS. The human-induced TWS variations in the Yangtze River basin have been preliminarily estimated from GRACE remotely sensed data and LSM simulations over the 8 year period studied. GRACE detected TWS variations were affected by both climate variability and human interference, whereas the LSMs we used in this study simulated only the natural part of TWS variations taking no account of human activities. Without consideration of the feedback between human water use and terrestrial water fluxes, the human-induced TWS variations can thus be inferred from GRACE data by isolating the LSM-simulated TWS, given auxiliary information on the other components of TWS.

Two sets of LSM-simulated TWS data were used in this study, one was simulated by Noah-MP and driven by the ITPCAS meteorological data, and the other used ERA-Interim/Land. GRACE senses all phases of water stored above and below the surface of the Earth, and hence the GRACE-observed TWS variations include the combined contributions of SM, canopy water storage, snow water equivalent, ice, biomass, surface water and groundwater. The estimated TWS of both Noah-MP and ERA-Interim/Land, however, lacks certain components due to missing processes and storage parameters, although these differ for the two. More specifically, the Noah-MP-estimated TWS only includes SM, canopy water storage, snow water equivalent, and groundwater, whereas the estimated TWS from ERA-Interim/Land is limited to SM and snow water equivalent. Ice and biomass account for a tiny percentage of TWS in the Yangtze River basin, and thus have negligible impacts on TWS variations [*Yang et al*., 2011]. Compared to the Noah-MP-simulated TWS, canopy water storage and groundwater components are missing in the ERA-Interim/Land-produced TWS. However, canopy water storage in the Yangtze River basin is negligible in comparison with SM [*Yang et al*., 2011], thereby having little impact on TWS variations. Moreover, the ERA-Interim/Land model, HTESSEL, has a deep soil reservoir to mimic shallow groundwater storage variations to take into account a capillary connection between groundwater and evaporation to avoid warm biases. Consequently, the estimated TWS from ERA-Interim/Land to some extent reflects the groundwater variations, although it does not explicitly model

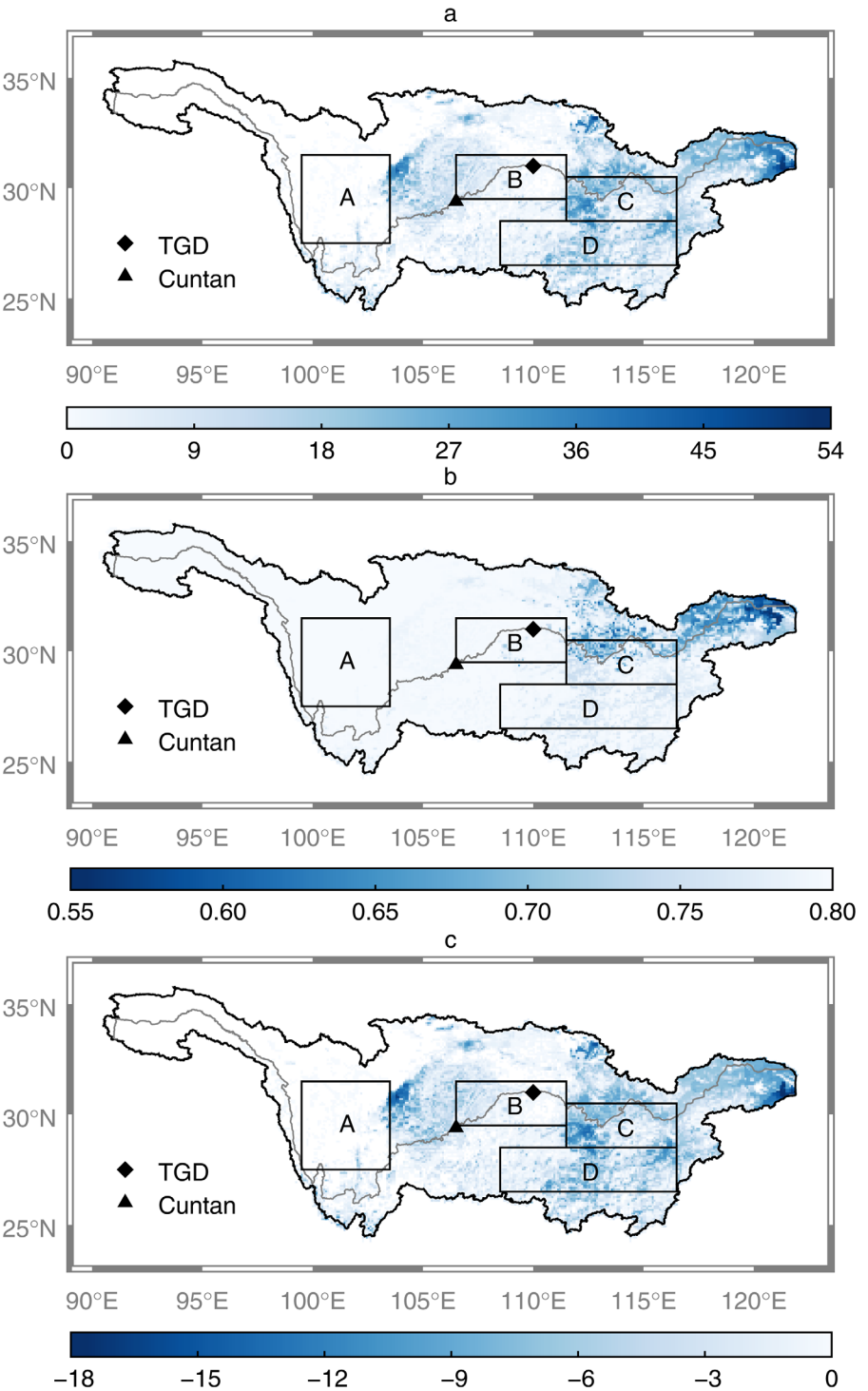

Figure 7. (a) Actually irrigated area, in km^2, (b) fraction of return flows f_{rgi} from irrigation to groundwater, and (c) yearly average net abstraction of groundwater NA_g, in cm yr^{-1}, for the period 2005–2010, with the spatial resolution of 5 min. Negative net abstraction of groundwater indicates groundwater storage gains.

groundwater [*Balsamo et al.*, 2009]. Furthermore, missing or poor model representations of, for instance, snow, surface water bodies, and groundwater predominantly affect the amplitudes of seasonal variations in TWS rather than natural interannual trends [*Swenson and Milly*, 2006; *Syed et al.*, 2008]. This is due to the fact that the physical consistency (i.e., closure of the water and energy budgets) is maintained by

Table 2. The Human-Induced Net Groundwater Gain ($-NA_g$) and Groundwater Recharge, Calculated Using the Method of *Döll et al.* [2012] in Regions A–D[a]

	Region A	Region B	Region C	Region D
$-NA_g$	0.2	1.2	4.2	3.0
Groundwater recharge	0.3	1.5	5.2	3.6
GRACE-Noah-MP	−0.5	1.1	3.7	1.9
GRACE-ERA-Interim/Land	−0.7	1.3	3.9	1.4

[a]It should be noted that, in order to facilitate a comparison of the alternative estimates, the increments in the estimated human-induced TWS based on GRACE and LSMs (Figure 6) are also shown here. Unit: cm yr^{-1}.

constructing in LSMs, and hence the LSM-simulated TWS can largely represent the natural variability of meteorological fields.

Since simulated TWS from the LSMs does not account for all the components of TWS (e.g., surface water storage component), which is contrary to GRACE-derived TWS, our proposed method to estimate the human impacts is recommended for catchments with negligible changes in those components. Moreover, the use of two models is supported by the current developments in LSMs, whereby ensemble models are employed to average bias [*Yang et al.*, 2011]. Although these models have their own limitations, and using only two models does not necessarily reduce the errors, the comparable simulations from two validated models may improve our confidence in the obtained natural variability of TWS.

As shown in Figure 4, both the trends in estimated human-induced TWS variations from GRACE-Noah-MP (Figure 4a) and from GRACE-ERA-Interim/Land (Figure 4b) show very similar patterns to GRACE (Figure 4c), which illustrates that neither LSM-simulated TWS exhibits significant trends during the study period. This demonstrates that the estimated human-induced TWS trends were not mathematical artifacts caused by subtraction of large negative LSM-simulated TWS trends from GRACE TWS trends and indicates that TWS trends, mainly originated from the GRACE solutions, were very likely caused by anthropogenic modification to the hydrological cycle rather than natural climate variability.

The estimated human-induced TWS changes from GRACE and LSMs can be validated by quantifying the impacts of water uses on surface and groundwater. The Yangtze River basin involves intensive human activities, such as irrigation and dam construction. The basin is rich in surface water with approximately 95% of the water supply originating from surface water, while the other 5% is from groundwater (Table 1). Water used for irrigation takes up a large amount of water supply and accounts for more than 50% (around 94.8×10^9 m^3) of total water use. The irrigated water is partly consumed by ET and outflow to the surface water bodies, whereas the other part recharges groundwater. Approximately 57.4×10^9 m^3 of water was available to return to surface and groundwater storage per year (Table 1), with 55%–80% recharging groundwater (Figure 7b). Due to irrigation, the mean net groundwater gain was nearly 36.8×10^9 m^3 (Table 1). As shown in Figure 7c, the middle and lower reaches of the basin experience large amounts of net groundwater gain due to irrigation. The spatial pattern of net abstraction/gain of groundwater matches the pattern of estimated human-induced TWS changes based on GRACE and LSMs well (Figure 4).

Four ROHs (Regions A, B, C, and D) within the study area were chosen based on TWS growth rates (Figure 4) for further examination and comparison. It should be noted that Region B is the hydraulic basin of the TGR, and that we selected this region to quantify the impacts of TGR impoundment on TWS changes. As shown in Figure 6, Region C experienced dramatic human-induced TWS increment at a mean rate of 3.7 ± 0.8 cm yr^{-1} estimated from GRACE and Noah-MP, and a rate of 3.9 ± 1.1 cm yr^{-1} estimated from GRACE and ERA-Interim/Land, respectively. Regions B and D also show positive human-induced TWS trends, although less than Region C, while Region A exhibits no significant trend. This is consistent with the yearly average net gain of groundwater, estimated based on the method of *Döll et al.* [2012] (Table 2): 0.2, 1.2, 4.2, and 3.0 cm yr^{-1} added to groundwater storage in Regions A, B, C, and D, respectively. The quantification of the impact of water use on groundwater storage, based on the method of *Döll et al.* [2012], is fully independent of the human-induced estimates from GRACE and LSMs, thus the high consistency between these methods verifies the estimated values and patterns of human-induced TWS, and also indicates that groundwater recharge from intensive surface water irrigation is an important contributor to the TWS increases in Regions B, C, and D.

Surface water storage (e.g., lakes, rivers) merits consideration. As shown in Figure 3, the monthly discharge from the main hydrological gauging stations (Cuntan, Yichang, and Datong) and from model simulations on the Yangtze River mainstream is rather stationary except in 2006. Similarly, it can be clearly seen from Figure 8 that no trends are exhibited in water level variations for the three largest natural lakes (Dongting Lake, Poyang Lake, and Tai Lake), provided by HYDROWEB during the study period. In combination with the

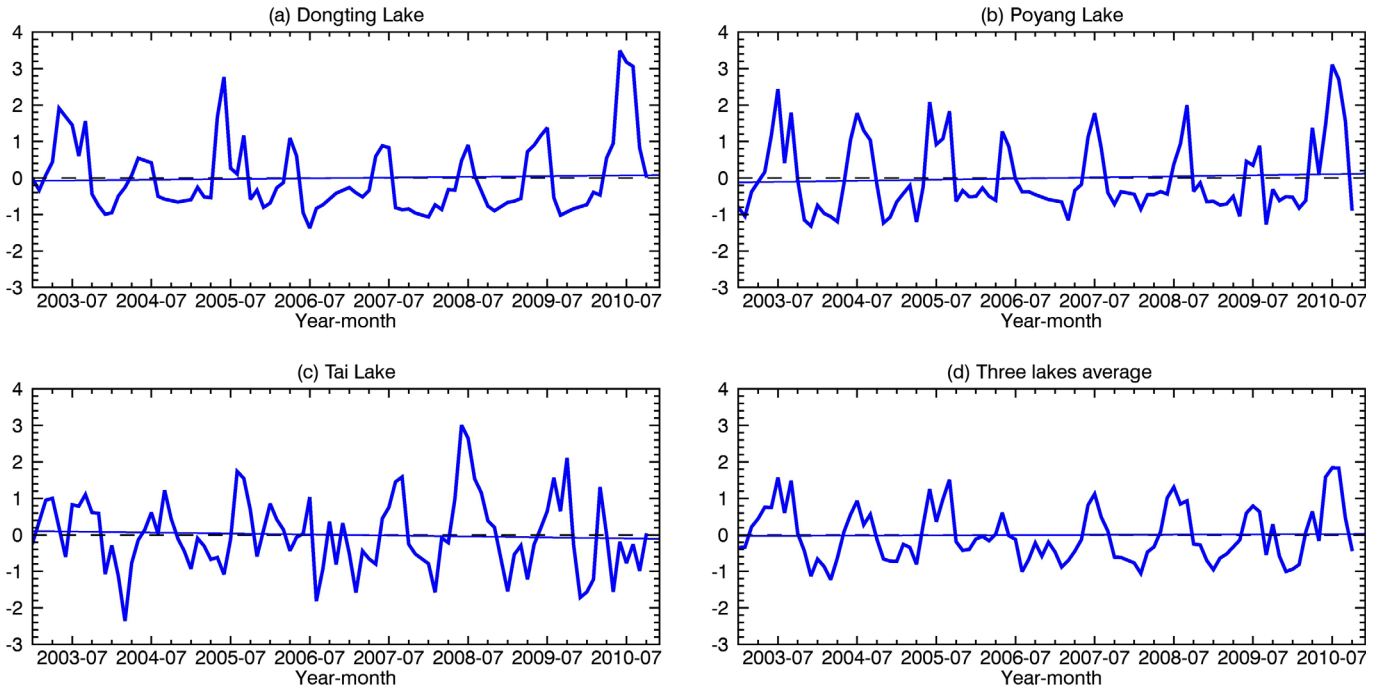

Figure 8. Monthly anomalies of water level (curve) and trends (line), during the study period, for (a) Donging Lake, (b) Poyang Lake, (c) Tai Lake, and (d) the three lakes' average, respectively. Unit: m.

information that there was no rise in the water surface areas of Dongting Lake and Poyang Lake estimated from remotely sensed data [*Hervé et al*., 2011], we can infer that the lake volumes of Dongting Lake and Poyang Lake did not experience positive trends during the study period. It should be noted that these two lakes, Dongting Lake and Poyang Lake, are located in Region C (Figure 2). Therefore, rivers and natural lakes did not contribute to the GRACE-observed TWS trends in the Yangtze River basin, at least in Region C, during the study period.

Groundwater and surface water are physically connected by the hydrologic cycle, and their interactions depend on the physiographic and climatic setting of the landscape. Due to the fact that these interactions take many forms, and so far have not been well investigated in the Yangtze River basin, we cannot elaborate on the processes of groundwater and surface water interaction. However, it is reasonable that the surface water bodies exhibited no trends while groundwater was continually increasing, because, first of all, the interannual changes in surface water bodies may not be sufficiently sensitive to changes in groundwater, as water that recharges groundwater originally comes from the surface water bodies. Second, the surface water bodies may gain water from inflow of groundwater in some stream reaches and lose water in other reaches, depending on the comparison between the altitude of the water table in the vicinity of streams and the altitude of the stream water surface. Third, in some regions, the groundwater system may be disconnected from streams by an unsaturated zone, where changes in groundwater storage do not affect the flow of streams [*Winter et al*., 1998].

Groundwater flow is much slower than riverine flows, thus the part of irrigated water that recharges groundwater can accumulate underground. Therefore, the GRACE-derived TWS (Figure 4c) was continuously increasing. It should be noted that Figure 6 shows a decline in the GRACE-derived and human-induced TWS during 2006, which is inconsistent with the estimates based on the method of *Döll et al*. [2012]. More specifically, the GRACE-derived TWS decreased by 3.7 cm on average in Region B and 6.7 cm in Region C in 2006 relative to the previous year 2005, whereas the estimated human-induced net groundwater gains were 1.2 cm in Region B and 4.2 cm in Region C (Table 2). This inconsistency can be explained by the 2006 extreme drought. As previously mentioned, an extreme drought occurred in 2006 in the Yangtze River basin. *Dai et al*. [2010] have shown that groundwater discharge along the middle and lower reaches plays an important role in the compensation of runoff and river level reduction in drought years. The total groundwater discharge was found to account for 31% of the increased river discharge between

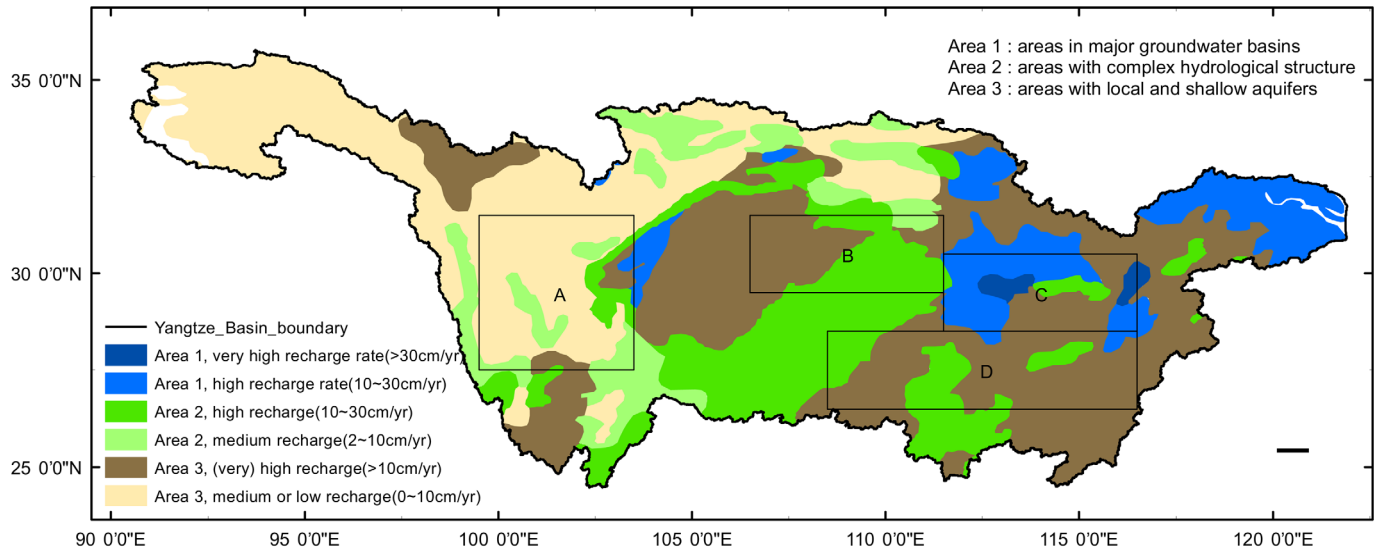

Figure 9. Groundwater resources map with aquifer systems in the Yangtze River basin [*WHYMAP*, 2008]. Blue, green, and brown colors represent the areas in major groundwater basins (Area 1), with complex hydrological structure (Area 2), and with local and shallow aquifers (Area 3), respectively. Light and dark colors represent the areas with relatively low and high recharge rate.

Yichang and Datong in 2006. However, the net abstractions of groundwater estimated from the method of *Döll et al*. [2012] consider no such compensation. It is also interesting that the net groundwater gain is very high in the Yangtze delta (Figure 7c), which is not captured by GRACE data (Figure 4). This might be due to the fact that the Yangtze delta was formed by a series of Chenier shell ridges that gradually extended the deltaic plain seaward through the sedimentary deposition of the Yangtze River, and that groundwater flow rates are relatively high in these high-permeability materials. The net gain of groundwater, thus, very likely flows away from the delta to neighboring regions.

There are other factors that were not considered in the quantification of net groundwater recharge. First, the underlying soil and geology may partly explain the differences in groundwater variations between the four regions. As shown in Figure 9, Region C is largely underlain by a major groundwater basin, with a high available recharge rate of 10–30 cm yr^{-1} or a very high recharge rate of more than 30 cm yr^{-1}. Regions B and D, located in areas with local and shallow aquifers or complex aquifers, also have a high recharge rate of 10–30 cm yr^{-1}. In contrast, Region A has a relatively low groundwater recharge rate of less than 10 cm yr^{-1} [*WHYMAP*, 2008]. The groundwater replenishment in Regions B, C, and D, thus, occurs easily when there is a water surplus, particularly in Region C. Second, the decrease of NDVI (Figure 10) in Regions B, C, and D indicates deterioration of the vegetation during the study period. The importance of vegetation in controlling water recharge in a natural system has been illustrated by previous studies [*Wang et al*., 2004; *Scanlon et al*., 2005, 2006], which show that changing land cover from vegetated to nonvegetated conditions increases groundwater recharge, as the decrease of vegetation cover reduces the ability of soil to retain water for plant use. This is consistent with the results that Regions B, C, and D had a decrease in NDVI but an increase in groundwater storage. All of the above implies that the intensive surface water irrigation, leading to groundwater gains, forms a main contributor to the GRACE-derived TWS trends in the middle and lower reaches of the Yangtze River basin.

Water impoundment in reservoirs can cause a large mass redistribution. *Wang et al*. [2011] proved that the water storage changes in the TGR can be captured by GRACE, which explains 76% of the monthly variability in in situ measurements. Thus, the GRACE-derived TWS trend in Region B, where the TGR is located, was also affected by the TGR operations. The impounded water volume of the TGR was 11.6, 5.6, and 6.1 km^3 during the first filling stage in June 2003, the second filling stage in 2006, and the third filling stage in 2008, respectively. Due to the TGR impoundment, Region B experienced a TWS increment at a mean rate of 0.3 cm yr^{-1} during the study period, as calculated by adding up the impounded water volumes of all three filling stages (23.3 km^3) and dividing this figure by the area of Region B (about 1×10^5 km^2) and the value of 8 (for the 8 year period). This value of 0.3 cm yr^{-1} is relatively small (24%) compared to the net groundwater gain

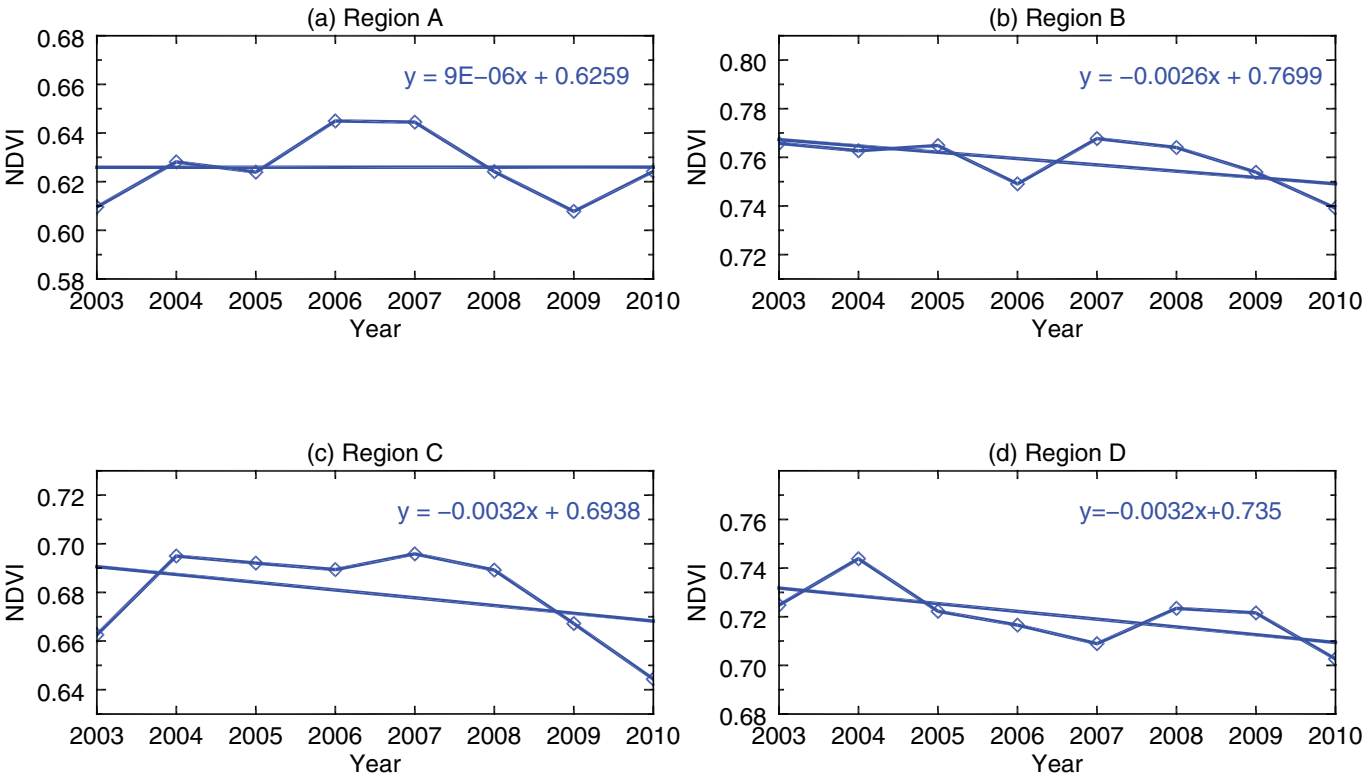

Figure 10. Spatial averaged annual NDVI changes (diamond curve) in summer and associated trends (line), during the study period, in Regions A–D.

($-NA_g$) in Region B (1.2 cm yr^{-1}). Considering both water impoundment in the TGR and net groundwater gain due to irrigation, the total annual TWS trend of Region B amounts to 1.5 cm yr^{-1}. This value is within the range of human-induced TWS changes estimated from GRACE-Noah-MP (1.1 $\pm$ 1.1 cm yr^{-1}), and the estimate from GRACE-ERA-Interim/Land (1.3 $\pm$ 0.6 cm yr^{-1}). The TGR water impoundment, thus, accounted for nearly 20% of the human-induced TWS changes. However, Region B, where the TGR is located, exhibits a less significant trend than Region C does. This indicates that water impoundment in reservoirs is an important contributor, but not the dominant one to the large-scale TWS changes in the Yangtze River basin.

The feedback between human water use and terrestrial water fluxes needs careful consideration. On the one hand, human water use is influenced by climate variation. When using equation (1) to estimate the human-induced TWS changes, it includes the uncertainties caused by the influences of climate variation on human water use. Climate variability may change, for instance, irrigation water demand, and consequently change water use and withdrawal. The stable climate during the study period, however, does not cause big changes in water use and can largely reduce the uncertainties. As mentioned previously, the climate in the Yangtze River basin has been relatively stationary for the period 2003–2010. As a result, the changes in water use caused by climate variability are small, which can also be confirmed by the small changes in irrigation water use data, as listed in Table 1. Therefore, the associated discrepancy between the estimated human-induced TWS changes and the actual values is small. On the other hand, climate variation is influenced by human water use. As previously mentioned, the Yangtze River basin, especially the middle and lower reaches, is dominated by the ET demand limited regime, where terrestrial water fluxes are mainly controlled by net radiation rather than SM. Hence, human water use such as irrigation causes changes in SM but has little influence on climate variation.

7. Conclusions

In this study, we proposed a framework for detection and attribution of spatial TWS changes. This framework integrates GRACE satellite detection and macroscale hydrological models and gives water managers/researchers a useful tool to investigate the spatial human effects on TWS in various climate regimes.

Moreover, this proposed framework provides valuable insights for regions where in situ data are inaccessible. For regions with some in situ data of, for instance, groundwater levels, it is recommended to use data assimilation, which can combine the virtues of in situ data and hydrological modeling, rather than solely use point measurements, to validate GRACE satellite estimates. Furthermore, the framework takes into account the feedback between human water use and terrestrial water fluxes and stresses the importance of selecting a climate stationary period as the study period and, based on SM-climate interactions, of choosing a suitable hydrological model to validate the GRACE detection, which is very different from previous GRACE applications [e.g., *Rodell et al*., 2009; *Feng et al*., 2013; *Voss et al*., 2013].

This framework is illustrated by its application to the Yangtze River basin, due to the fact that GRACE data have rarely been applied in a water-rich basin to estimate spatial effects of human-induced changes on TWS mainly caused by large-scale irrigation. For this basin, we conclude that the spatial pattern of TWS, especially in the middle and lower reaches, was changing during the period 2003–2010, and this change was occurring as a result of anthropogenic modification to the hydrological cycle rather than natural climate variability. Human activity such as intensive surface water irrigation and reservoir operation was increasing the TWS continuously in the middle and lower reaches, as was captured by subtracting LSM simulations from GRACE satellite data. This human-induced increase in TWS was mainly attributed to intensive surface water irrigation, which leads to groundwater gains. The TGR impoundment was also a noticeable cause for TWS changes in the reservoir region and accounted for nearly 20% of the human-induced TWS increment. However, we should acknowledge the shortcomings, such as the absence of groundwater measurements and detailed information on reservoirs construction and management in the case study.

Although there is no substitute for ground-based observational data, emerging advances in hydrologic remote sensing and hydrological models, combined with better understanding of the hydrologic cycle, allow us to gradually break the limit of in situ data unavailability and construct a holistic picture of changing water availability for a particular region or across the globe. In this study, the proposed framework for detection of human-induced changes to TWS reflects that science-informed perspective.

Acknowledgments

This research was funded in part by the ESA-MOST Dragon III programme: Concerted Earth Observation and Prediction of Water and Energy Cycles in the Third Pole Environment (CEOP-TPE). Ying Huang was supported by the Chinese Scholarship Council (CSC). We are grateful to the editors and reviewers for their valuable comments and constructive suggestions, which have greatly assisted us in improving the quality of the paper. Moreover, we thank all the researchers who processed RL05 GRACE L2 product in the Center for Space Research(CSR) at the University of Texas at Austin, USA, and Jet Propulsion Laboratory(JPL), NASA, USA, which are freely available at the website ftp://podaac-ftp.jpl.nasa.gov/allData/tellus/L3/land_mass/RL05/netcdf/. The atmospheric forcing data provided by the Institute of Tibetan Plateau Research, Chinese Academy of Sciences (ITPCAS), which can be obtained from http://westdc.westgis.ac.cn/data/7a35329c-c53f-4267-aa07-e0037d913a21; ERA-Interim/Land product provided by European Center for Medium-Range Weather Forecasts (ECMWF), which can be obtained from http://apps.ecmwf.int/datasets/data/interim_land/; HYDROWEB provided by Laboratoire d'Etude en Géophysique et Océanographie Spatiale (LEGOS), which is available at http://www.legos.obs-mip.fr/en/soa/hydrologie/hydroweb/. The Moderate Resolution Imaging Spectroradiometer (MODIS) product provided by U.S. Geological Survey (USGS), which can be obtained from https://lpdaac.usgs.gov/products/modis_products_table. The Global Land Data Assimilation System (GLDAS) product provided by NASA, USA, which is available at http://ldas.gsfc.nasa.gov/gldas/. The water withdrawal and uses data from the Ministry of Water Resources of the People's Republic of China (P.R. China), which is available at http://www.mwr.gov.cn/zwzc/hygb/szygb/. Observed discharge data are obtained from http://219.140.196.71/sq/data/sc.action?scid=cjh.sq.

References

Alcamo, J., P. Döll, T. Henrichs, F. Kaspar, B. Lehner, T. Rösch, and S. Siebert (2003a), Development and testing of the WaterGAP 2 global model of water use and availability, *Hydrol. Sci. J.*, *48*(3), 317–337.

Alcamo, J., P. Döll, T. Henrichs, F. Kaspar, B. Lehner, T. Rösch, and S. Siebert (2003b), Global estimates of water withdrawals and availability under current and future business-as-usual conditions, *Hydrol. Sci. J.*, *48*(3), 339–348.

Ball, J. T., I. E. Woodrow, and J. A. Berry (1987), A model predicting stomatal conductance and its contribution to the control of photosynthesis under different environmental conditions, in *Process in Photosynthesis Research*, vol. 1, edited by J. Biggins, pp. 221–234, Martinus Nijhoff, Dordrecht, Netherlands.

Balsamo, G., A. Beljaars, K. Scipal, P. Viterbo, B. van den Hurk, M. Hirschi, and A. K. Betts (2009), A revised hydrology for the ECMWF model: Verification from field site to terrestrial water storage and impact in the integrated forecast system, *J. Hydrometeorol.*, *10*(3), 623–643.

Balsamo, G., et al. (2015), ERA-Interim/Land: A global land surface reanalysis data set, *Hydrol. Earth Syst. Sci.*, *19*(1), 389–407.

Barco, J., T. S. Hogue, M. Girotto, D. R. Kendall, and M. Putti (2010), Climate signal propagation in southern California aquifers, *Water Resour. Res.*, *46*, W00F05, doi:10.1029/2009WR008376.

Bonan, G. B. (1996), A land surface model (LSM version 1.0) for ecological, hydrological, and atmospheric studies: Technical description and user's guide, *NCAR Tech. Note NCAR/TN-417+STR*, 150 pp., Natl. Cent. for Atmos. Res., Boulder, Colo.

Chen, Y., K. Yang, J. He, J. Qin, J. Shi, J. Du, and Q. He (2011), Improving land surface temperature modeling for dry land of China, *J. Geophys. Res.*, *116*, D20104, doi:10.1029/2011JD015921.

Collatz, G. J., J. T. Ball, C. Grivet, and J. A. Berry (1991), Physiological and environmental regulation of stomatal conductance, photosynthesis and transpiration: A model that includes a laminar boundary layer, *Agric. For. Meteorol.*, *54*(24), 107–136.

Collatz, G. J., M. Ribascarbo, and J. A. Berry (1992), A coupled photosynthesis-stomatal conductance model for leaves of C4 plants, *Aust. J. Plant Physiol.*, *19*, 519–538, doi:10.1071/PP9920519.

Crétaux, J. F., et al. (2011), SOLS: A lake database to monitor in the Near Real Time water level and storage variations from remote sensing data, *Adv. Space Res.*, *47*(9), 1497–1507.

Dai, Z.-j., J.-z. Du, A. Chu, J.-f. Li, J.-y. Chen, and X.-l. Zhang (2010), Groundwater discharge to the Changjiang River, China, during the drought season of 2006: Effects of the extreme drought and the impoundment of the Three Gorges Dam, *Hydrogeol. J.*, *18*(2), 359–369.

Dee, D. P., et al. (2011), The ERA-Interim reanalysis: Configuration and performance of the data assimilation system, *Q. J. R. Meteorol. Soc.*, *137*(656), 553–597.

Döll, P., K. Fiedler, and J. Zhang (2009), Global-scale analysis of river flow alterations due to water withdrawals and reservoirs, *Hydrol. Earth Syst. Sci.*, *13*(12), 2413–2432.

Döll, P., H. Hoffmann-Dobrev, F. T. Portmann, S. Siebert, A. Eicker, M. Rodell, G. Strassberg, and B. R. Scanlon (2012), Impact of water withdrawals from groundwater and surface water on continental water storage variations, *J. Geodyn.*, *5960*(0), 143–156.

Famiglietti, J. S., D. Ryu, A. A. Berg, M. Rodell, and T. J. Jackson (2008), Field observations of soil moisture variability across scales, *Water Resour. Res.*, *44*, W01423, doi:10.1029/2006WR005804.

Famiglietti, J. S., M. Lo, S. L. Ho, J. Bethune, K. J. Anderson, T. H. Syed, S. C. Swenson, C. R. de Linage, and M. Rodell (2011), Satellites measure recent rates of groundwater depletion in California's Central Valley, *Geophys. Res. Lett.*, *38*, L03403, doi:10.1029/2010GL046442.

Feick, S., S. Siebert, and P. Döll (2005), *A Digital Global Map of Artificially Drained Agricultural Areas*, *Frankfurt Hydrol. Pap. 04*, 57 pp., Inst. of Phys. Geogr., Univ. of Frankfurt, Frankfurt am Main, Germany.

Feng, W., M. Zhong, J.-M. Lemoine, R. Biancale, H.-T. Hsu, and J. Xia (2013), Evaluation of groundwater depletion in North China using the Gravity Recovery and Climate Experiment (GRACE) data and ground-based measurements, *Water Resour. Res.*, *49*, 2110–2118, doi: 10.1002/wrcr.20192.

Hanasaki, N., S. Kanae, T. Oki, K. Masuda, K. Motoya, N. Shirakawa, Y. Shen, and K. Tanaka (2008a), An integrated model for the assessment of global water resources. Part 1: Model description and input meteorological forcing, *Hydrol. Earth Syst. Sci.*, *12*(4), 1007–1025.

Hanasaki, N., S. Kanae, T. Oki, K. Masuda, K. Motoya, N. Shirakawa, Y. Shen, and K. Tanaka (2008b), An integrated model for the assessment of global water resources. Part 2: Applications and assessments, *Hydrol. Earth Syst. Sci.*, *12*(4), 1027–1037.

He, J. (2010), Development of surface meteorological dataset of China with high temporal and spatial resolution, MS thesis, Inst. of Tibetan Plateau Res., Chin. Acad. of Sci., Beijing, China.

Hervé, Y., et al. (2011), Nine years of water resources monitoring over the middle reaches of the Yangtze River, with ENVISAT, MODIS, Beijing-1 time series, Altimetric data and field measurements, *Lakes Reservoirs Res. Manage.*, *16*(3), 231–247.

Huang, Y., M. S. Salama, M. S. Krol, R. van der Velde, A. Y. Hoekstra, Y. Zhou, and Z. Su (2013), Analysis of long-term terrestrial water storage variations in the Yangtze River basin, *Hydrol. Earth Syst. Sci.*, *17*(5), 1985–2000.

IPCC (2012), *Managing the Risks of Extreme Events and Disasters to Advance Climate Change Adaptation. A Special Report of Working Groups I and II of the Intergovernmental Panel on Climate Change [Field, C.B., V. Barros, T.F. Stocker, D. Qin, D.J. Dokken, K.L. Ebi, M.D. Mastrandrea, K.J. Mach, G.-K. Plattner, S.K. Allen, M. Tignor, and P.M. Midgley (eds.)]*, 582 pp., Cambridge Univ. Press, Cambridge, U. K.

Jung, M., et al. (2010), Recent decline in the global land evapotranspiration trend due to limited moisture supply, *Nature*, *467*(7318), 951–954.

Kummu, M., P. J. Ward, H. de Moel, and O. Varis (2010), Is physical water scarcity a new phenomenon? Global assessment of water shortage over the last two millennia, *Environ. Res. Lett.*, *5*(3), 034006.

Landerer, F. W., and S. C. Swenson (2012), Accuracy of scaled GRACE terrestrial water storage estimates, *Water Resour. Res.*, *48*, W04531, doi:10.1029/2011WR011453.

Lo, M.-H., and J. S. Famiglietti (2013), Irrigation in California's Central Valley strengthens the southwestern U.S. water cycle, *Geophys. Res. Lett.*, *40*, 301–306, doi:10.1002/grl.50108.

Lorenzo-Lacruz, J., S. M. Vicente-Serrano, J. I. López-Moreno, S. Begueria, J. M. Garcia-Ruiz, and J. M. Cuadrat (2010), The impact of droughts and water management on various hydrological systems in the headwaters of the Tagus River (central Spain), *J. Hydrol.*, *386*(14), 13–26.

Long, D., Y. Yang, Y. Wada, Y. Hong, W. Liang, Y. Chen, B. Yong, A. Hou, J. Wei, L. Chen (2015), Deriving scaling factors using a global hydrological model to restore GRACE total water storage changes for China's Yangtze River Basin, *Remote Sens. Environ.*, *168*, 177–193.

Mair, A., and A. Fares (2010), Influence of groundwater pumping and rainfall spatio-temporal variation on streamflow, *J. Hydrol.*, *393*(34), 287–308.

Morrison, F. A. (2014), *Obtaining Uncertainty Measures on Slope and Intercept of a Least Squares Fit With Excels LINEST*, Mich. Technol. Univ., Houghton.

Niu, G.-Y., and Z.-L. Yang (2004), Effects of vegetation canopy processes on snow surface energy and mass balances, *J. Geophys. Res.*, *109*, D23111, doi:10.1029/2004JD004884.

Niu, G.-Y., and Z.-L. Yang (2006), Effects of frozen soil on snowmelt runoff and soil water storage at a continental scale, *J. Hydrometeorol.*, *7*(5), 937–952.

Niu, G.-Y., Z.-L. Yang, R. E. Dickinson, and L. E. Gulden (2005), A simple TOPMODEL-based runoff parameterization (SIMTOP) for use in global climate models, *J. Geophys. Res.*, *110*, D21106, doi:10.1029/2005JD006111.

Niu, G.-Y., Z.-L. Yang, R. E. Dickinson, L. E. Gulden, and H. Su (2007), Development of a simple groundwater model for use in climate models and evaluation with Gravity Recovery and Climate Experiment data, *J. Geophys. Res.*, *112*, D07103, doi:10.1029/2006JD007522.

Niu, G.-Y., et al. (2011), The community Noah land surface model with multiparameterization options (Noah-MP): 1. Model description and evaluation with local-scale measurements, *J. Geophys. Res.*, *116*, D12109, doi:10.1029/2010JD015139.

Pokhrel, Y., N. Hanasaki, S. Koirala, J. Cho, P. J. F. Yeh, H. Kim, S. Kanae, and T. Oki (2011), Incorporating anthropogenic water regulation modules into a land surface model, *J. Hydrometeorol.*, *13*(1), 255–269.

Rodell, M., et al. (2004), The Global Land Data Assimilation System, *Bull. Am. Meteorol. Soc.*, *85*(3), 381–394.

Rodell, M., I. Velicogna, and J. S. Famiglietti (2009), Satellite-based estimates of groundwater depletion in India, *Nature*, *460*(7258), 999–1002.

Rui, H. (2011), *README Document for Global Land Data Assimilation System Version 1 (GLDAS-1) Products*, Goddard Earth Sci. Data and Inf. Serv. Cent., NASA., Greenbelt, Md.

Ryu, Y., D. D. Baldocchi, S. Ma, and T. Hehn (2008), Interannual variability of evapotranspiration and energy exchange over an annual grassland in California, *J. Geophys. Res.*, *113*, D09104, doi:10.1029/2007JD009263.

Savenije, H. H. G., A. Y. Hoekstra, and P. van der Zaag (2014), Evolving water science in the Anthropocene, *Hydrol. Earth Syst. Sci.*, *18*(1), 319–332.

Scanlon, B. R., R. C. Reedy, D. A. Stonestrom, D. E. Prudic, and K. F. Dennehy (2005), Impact of land use and land cover change on groundwater recharge and quality in the southwestern US, *Global Change Biol.*, *11*(10), 1577–1593.

Scanlon, B. R., K. E. Keese, A. L. Flint, L. E. Flint, C. B. Gaye, W. M. Edmunds, and I. Simmers (2006), Global synthesis of groundwater recharge in semiarid and arid regions, *Hydrol. Processes*, *20*(15), 3335–3370.

Sellers, P. J., D. A. Randall, G. J. Collatz, J. A. Berry, C. B. Field, D. A. Dazlich, C. Zhang, G. D. Collelo, and L. Bounoua (1996), A revised land surface parameterization (SiB2) for atmospheric GCMS. Part I: Model formulation, *J. Clim.*, *9*(4), 676–705.

Seneviratne, S. I., and R. Stöckli (2008), The role of land-atmosphere interactions for climate variability in Europe, in *Climate Variability and Extremes During the Past 100 Years*, edited by S. Brönnimann et al., pp. 179–193, Springer, Dordrecht, Netherlands.

Seneviratne, S. I., T. Corti, E. L. Davin, M. Hirschi, E. B. Jaeger, I. Lehner, B. Orlowsky, and A. J. Teuling (2010), Investigating soil moisture–climate interactions in a changing climate: A review, *Earth Sci. Rev.*, *99*(34), 125–161.

Sheffield, J., G. Goteti, and E. F. Wood (2006), Development of a 50-year high-resolution global dataset of meteorological forcings for land surface modeling, *J. Clim.*, *19*(13), 3088–3111.

Siebert, S., P. Döll, J. Hoogeveen, J. M. Faures, K. Frenken, and S. Feick (2005), Development and validation of the global map of irrigation areas, *Hydrol. Earth Syst. Sci.*, *9*(5), 535–547.

Siebert, S., V. Henrich, K. Frenken, and J. Burke (2013), *Global Map of Irrigation Areas Version 5*, Rheinische Friedrich-Wilhelms-Univ., Bonn, Germany.

Smithson, P. A. (2002), IPCC, 2001: Climate change 2001: The scientific basis. Contribution of Working Group 1 to the Third Assessment Report of the Intergovernmental Panel on Climate Change, edited by J. T. Houghton, Y. Ding, D. J. Griggs, M. Noguer, P. J. van der

Linden, X. Dai, K. Maskell and C. A. Johnson (eds). Cambridge University Press, Cambridge, UK, and New York, USA, 2001. No. of pages: 881. Price £34.95, US$49.95, ISBN 0-521-01495-6 (paperback). £90.00, US$130.00, ISBN 0-521-80767-0 (hardback), *Int. J. Climatol.*, 22(9), 1144.

Swenson, S. C., and P. C. D. Milly (2006), Climate model biases in seasonality of continental water storage revealed by satellite gravimetry, *Water Resour. Res.*, *42*, W03201, doi:10.1029/2005WR004628.

Syed, T. H., J. S. Famiglietti, M. Rodell, J. Chen, and C. R. Wilson (2008), Analysis of terrestrial water storage changes from GRACE and GLDAS, *Water Resour. Res.*, *44*, W02433, doi:10.1029/2006WR005779.

Tapley, B. D., S. Bettadpur, J. C. Ries, P. F. Thompson, and M. M. Watkins (2004), GRACE measurements of mass variability in the earth system, *Science*, *305*(5683), 503–505.

Teuling, A. J., et al. (2009), A regional perspective on trends in continental evaporation, *Geophys. Res. Lett.*, *36*, L02404, doi:10.1029/2008GL036584.

Thomas, A. (2008), Agricultural irrigation demand under present and future climate scenarios in China, *Global Planet. Change*, *60*(34), 306–326.

van Beek, L. P. H., Y. Wada, and M. F. P. Bierkens (2011), Global monthly water stress: 1. Water balance and water availability, *Water Resour. Res.*, *47*, W07517, doi:10.1029/2010WR009791.

van den Hurk, B. J. J. M., P. Viterbo, A. C. M. Beljaars, and A. K. Betts (2000), Offline validation of the ERA40 surface scheme, *ECMWF Tech. Memo 295*, 43 pp., Eur. Cent. for Medium-Range Weather Forecasts, Reading, U. K. [Available at http://www.ecmwf.int/publications/library/ecpublications/_pdf/tm/001-300/tm295.pdf.]

van Loon, A. F., and H. A. J. van Lanen (2013), Making the distinction between water scarcity and drought using an observation-modeling framework, *Water Resour. Res.*, *49*, 1483–1502, doi:10.1002/wrcr.20147.

Viterbo, P., and A. C. M. Beljaars (1995), An improved land surface parameterization scheme in the ECMWF model and its validation, *J. Clim.*, *8*(11), 2716–2748.

Vörösmarty, C. J., et al. (2010), Global threats to human water security and river biodiversity, *Nature*, *467*(7315), 555–561.

Voss, K. A., J. S. Famiglietti, M. Lo, C. de Linage, M. Rodell, and S. C. Swenson (2013), Groundwater depletion in the Middle East from GRACE with implications for transboundary water management in the Tigris-Euphrates-Western Iran region, *Water Resour. Res.*, *49*, 904–914, doi:10.1002/wrcr.20078.

Wada, Y., D. Wisser, and M. F. P. Bierkens (2014), Global modeling of withdrawal, allocation and consumptive use of surface water and groundwater resources, *Earth Syst. Dyn.*, *5*(1), 15–40.

Wada, Y., L. P. H. van Beek, C. M. van Kempen, J. W. T. M. Reckman, S. Vasak, and M. F. P. Bierkens (2010), Global depletion of groundwater resources, *Geophys. Res. Lett.*, *37*, L20402, doi:10.1029/2010GL044571.

Wada, Y., L. P. H. van Beek, and M. F. P. Bierkens (2011a), Modelling global water stress of the recent past: On the relative importance of trends in water demand and climate variability, *Hydrol. Earth Syst. Sci.*, *15*(12), 3785–3808.

Wada, Y., L. P. H. van Beek, D. Viviroli, H. H. Dürr, R. Weingartner, and M. F. P. Bierkens (2011b), Global monthly water stress: 2. Water demand and severity of water stress, *Water Resour. Res.*, *47*, W07518, doi:10.1029/2010WR009792.

Wang, X., C. de Linage, J. Famiglietti, and C. S. Zender (2011), Gravity Recovery and Climate Experiment (GRACE) detection of water storage changes in the Three Gorges Reservoir of China and comparison with in situ measurements, *Water Resour. Res.*, *47*, W12502, doi:10.1029/2011WR010534.

Wang, X.-P., R. Berndtsson, X.-R. Li, and E.-S. Kang (2004), Water balance change for a re-vegetated xerophyte shrub area [Changement du bilan hydrique d'une zone replantée d'arbustes xérophiles], *Hydrol. Sci. J.*, *49*(2), 283–295.

WHYMAP (2008), World-wide Hydrogeological Mapping and Assessment Programme, in *Groundwater Resources of the World*, scale 1: 25,000,000, BGR/UNESCO, Hannover, Germany.

Winter, T. C., J. W. Harvey, O. L. Franke, and W. M. Alley (1998), Ground water and surface water: A single resource, *U.S. Geol. Surv. Circ.*, *1139*, 2–21.

Wisser, D., S. Frolking, E. M. Douglas, B. M. Fekete, C. J. Vörösmarty, and A. H. Schumann (2008), Global irrigation water demand: Variability and uncertainties arising from agricultural and climate data sets, *Geophys. Res. Lett.*, *35*, L24408, doi:10.1029/2008GL035296.

Yang, R., and M. A. Friedl (2003), Modeling the effects of three-dimensional vegetation structure on surface radiation and energy balance in boreal forests, *J. Geophys. Res.*, *108*(D16), 8615, doi:10.1029/2002JD003109.

Yang, Z.-L., et al. (2011), The community Noah land surface model with multiparameterization options (Noah-MP): 2. Evaluation over global river basins, *J. Geophys. Res.*, *116*, D12110, doi:10.1029/2010JD015140.

Zaitchik, B. F., A. K. Macalady, L. R. Bonneau, and R. B. Smith (2006), Europe's 2003 heat wave: A satellite view of impacts and land–atmosphere feedbacks, *Int. J. Climatol.*, *26*(6), 743–769.

Zhang, L., W. R. Dawes, and G. R. Walker (2001), Response of mean annual evapotranspiration to vegetation changes at catchment scale, *Water Resour. Res.*, *37*(3), 701–708.

Zhang, Z., B. F. Chao, J. Chen, and C. R. Wilson (2015), Terrestrial water storage anomalies of Yangtze River Basin droughts observed by GRACE and connections with ENSO, *Global Planet. Change*, *126*(0), 35–45.